ISSN 1340-3745

ICRR-Report-463-2000-7

Observation of Atmospheric Neutrinos

Takaaki Kajita and Yoji Totsuka

(August 2000)

Submitted to Reviews of Modern Physics

INSTITUTE FOR COSMIC RAY RESEARCH
UNIVERSITY OF TOKYO

Observation of atmospheric neutrinos

Takaaki Kajita[a] and Yoji Totsuka[b]
[a]Research Center for Cosmic Neutrinos, Institute for Cosmic Ray Research, University of Tokyo
5-1-5 Kashiwa-no-ha, Kashiwa, Chiba 227-8582, Japan
[b]Kamioka Observatory, Institute for Cosmic Ray Research, University of Tokyo
Higashi-Mozumi, Kamioka-cho, Gifu, 506-1205, Japan

Atmospheric neutrinos are produced as decay products in hadronic showers resulting from collisions of cosmic rays with nuclei in the atmosphere. Electron neutrinos and muon neutrinos are produced mainly by the decay chain of charged pions to muons to electrons. Atmospheric neutrinos have been observed by large underground detectors. Depending on the energy of the neutrinos, atmospheric neutrinos are observed as fully-contained events, partially contained events or upward-going muon events. The energy range covered by these events is from a few hundred MeV to above 100 GeV. It has been known for about ten years that some data suggested the existence of neutrino oscillations. With the recent increase of event statistics, especially from the Super-Kamiokande data, the atmospheric neutrino data gave evidence for neutrino oscillations. Two-flavor $\nu_\mu \to \nu_\tau$ oscillations, with $\sin^2 2\theta > 0.88$ and Δm^2 in the region of 2×10^{-3} to 5×10^{-3} eV^2, explain all these data.

CONTENTS

I. INTRODUCTION AND HISTORY

Studies of the neutrino have played essential roles in the understanding of elementary particle physics. In the standard model of elementary particle physics, the neutrino has been assumed to have no electric charge, interact with other particles only via weak interactions, and have zero mass. In the 1970's, there was important theoretical progress. One advance was the development of Grand Unified Theories (GUTs) of strong, weak and electromagnetic interactions (Pati and Salam, 1973; Georgi and Glashow, 1974). In many non-minimal versions of GUT models, the neutrino masses are suggested to be non-zero (for a review, see for example, Langacker, 1981). The other advance was the seesaw mechanism (Yanagida, 1979; Gell-Mann, Ramond, Slansky, 1979) which naturally explains the smallness of the neutrino masses. Through these developments, the importance of renewed experimental searches for neutrino mass was recognized.

A sensitive way to observe small neutrino masses is to study neutrino flavor oscillations (Maki, Nakagawa, Sakata, 1962; Nakagawa *et al.*, 1963; Pontecorvo, 1967; Gribov and Pontecorvo, 1969; see also, Pontecorvo, 1957). For simplicity, we consider a two-neutrino oscillation hypothesis. If the neutrinos are massive, the flavor eigenstates, ν_α and ν_β, are expressed as combinations of mass eigenstates, ν_i and ν_j:

$$\begin{pmatrix} \nu_\alpha \\ \nu_\beta \end{pmatrix} = \begin{pmatrix} \cos\theta & \sin\theta \\ -\sin\theta & \cos\theta \end{pmatrix} \begin{pmatrix} \nu_i \\ \nu_j \end{pmatrix}, \tag{1}$$

where θ is the mixing angle between the flavor eigenstates and the mass eigenstates. The probability for a neutrino produced in a flavor state ν_α to be observed in a flavor state ν_β after traveling a distance L through a vacuum is:

$$P(\nu_\alpha \to \nu_\beta) = \sin^2 2\theta \sin^2\left(\frac{1.27\Delta m^2(\mathrm{eV}^2)L(\mathrm{km})}{E_\nu(\mathrm{GeV})}\right), \tag{2}$$

where E_ν is the neutrino energy and Δm^2 is the mass-squared difference of the neutrino mass eigenstates: $\Delta m^2 = m_j^2 - m_i^2$, where $m_{i(j)}$ represents the mass of $\nu_{i(j)}$. (The neutrino oscillation probability described in the above equation does not depend on the sign of Δm^2. Therefore, if the sign is not mentioned explicitly, we assume $\Delta m^2 > 0$ in this article.)

Over the past two decades, many reactor and accelerator experiments have searched for neutrino oscillations (for a review, see for example, Particle Data Group, 1998). In a nuclear reactor, low-energy ($\lesssim$10 MeV) $\overline{\nu}_e$'s are produced. Neutrino oscillations, $\overline{\nu}_e \to \overline{\nu}_x$, where $\overline{\nu}_x$ could be either $\overline{\nu}_\mu$ or $\overline{\nu}_\tau$, have been studied by searching for the disappearance of the $\overline{\nu}_e$ flux. No evidence for neutrino oscillations has been observed in these experiments. Two long baseline ($L \simeq 1$ km) reactor experiments (Apollonio *et al.*, 1998, 1999; Boehm *et al.*, 2000) excluded $\overline{\nu}_e \to \overline{\nu}_x$ oscillations with $\Delta m^2 \gtrsim 10^{-3}$ eV^2 for maximal mixing. These reactor experiments are sensitive to the values of $\sin^2 2\theta$ (for large Δm^2) down to about 0.1.

Accelerator neutrino oscillation experiments have searched for both $\nu_\mu \to \nu_e$ and $\nu_\mu \to \nu_x$ oscillations. In many of these experiments, a high energy ν_μ beam is used. As of this writing, only the LSND experiment (Athanassopoulos *et al.*, 1995, 1996a, 1996b, 1998) has observed evidence for $\nu_\mu \to \nu_e$ neutrino oscillations. The suggested region of neutrino oscillation parameters (Δm^2 and $\sin^2 2\theta$) from LSND (which has not been excluded by any other experiments) is between 0.2 and 2 eV^2 for Δm^2 and between 2×10^{-3} and 4×10^{-2} for $\sin^2 2\theta$. However, the situation is still controversial, because the KARMEN experiment (Steidl *et al.*, 1999; Jannakos *et al.*, 1999), which had a similar beam, neutrino flight distance and detector performance, has not observed any neutrino oscillation signal. Accelerator experiments have excluded $\Delta m^2 \gtrsim 10^{-1}$ eV^2 at maximal mixing (Borodovsky *et al.*, 1992; Steidl *et al.*, 1999, Jannakos *et al.*, 1999) and $\sin^2 2\theta \gtrsim 2 \times 10^{-3}$ eV^2 at large Δm^2 (Romosan *et al.*, 1997; Steidl *et al.*, 1999, Jannakos *et al.*, 1999) for $\nu_\mu \to \nu_e$ oscillations, and $\Delta m^2 \gtrsim 0.3$ eV^2 at maximal mixing (Dydak *et al.*, 1984; Bergsma *et al.*, 1984) and $\sin^2 2\theta \gtrsim 10^{-3}$ eV^2 at large Δm^2 (Astier *et al.*, 1999; Eskut *et al.*, 1998) for $\nu_\mu \to \nu_\tau$ (or $\nu_\mu \to \nu_x$) oscillations.

The Sun is a strong source of ν_e which are produced by nuclear fusion processes in its central region. These neutrinos are called solar neutrinos. To date, there have been five experiments which have observed solar neutrinos (Cleveland *et al.*, 1998; Fukuda *et al.*, 1996a; Abdurashitov *et al.*, 1999; Hampel *et al.*, 1999; Fukuda *et al.*, 1998). A deficit of the solar ν_e flux has been observed in all of these experiments. The observed fluxes are 30 to 60% of the solar model prediction (Bahcall, Basu and Pinsonneault, 1998) depending on the experiment. It is known that reasonable modifications of the solar model are unlikely to explain the present solar neutrino data. On the other hand, it is possible to explain the solar neutrino data by neutrino oscillations. The data suggest $\nu_e \to \nu_x$ neutrino oscillations. There are four consistent parameter regions of neutrino oscillations (see for example; Bahcall, Krastev and Smirnov, 1998): $10^{-5} \lesssim \Delta m^2 \lesssim 10^{-4}$ eV^2 and large $\sin^2 2\theta$, $\Delta m^2 \sim 10^{-5}$ eV^2 and $\sin^2 2\theta \sim 10^{-3}$, $\Delta m^2 \sim 10^{-7}$ eV^2 and large

$\sin^2 2\theta$, and $10^{-10} \lesssim \Delta m^2 \lesssim 10^{-9}$ eV^2 and large $\sin^2 2\theta$. One of the motivations of present and future solar neutrino experiments (McDonald, 1998; Oberauer, 1998; Lanou Jr., 1998) is to obtain conclusive evidence for solar neutrino oscillations and to determine the allowed parameter regions uniquely.

The atmospheric neutrino data which will be discussed in this article give evidence for neutrino oscillations between $\nu_\mu \to \nu_\tau$ with $10^{-3} \lesssim \Delta m^2 \lesssim 10^{-2}$ eV^2 and almost maximal mixing. To date, there has been no neutrino oscillation result which has contradicted the neutrino oscillation parameters obtained by the atmospheric neutrino data.

Cosmic ray interactions in the atmosphere produce neutrinos. These neutrinos are called atmospheric neutrinos. Atmospheric neutrinos arise from the decay of secondary particles (π, K and μ) produced by primary cosmic-ray interactions in the atmosphere. Typical altitudes of production of the neutrinos are between 10 and 20 km. These neutrinos can be detected by large underground detectors.

Atmospheric neutrino experiments started in the 1960's. One experiment was carried out in the Kolar Gold Field in South India (Achar *et al.*, 1965a, 1965b; Krishnaswamy *et al.*, 1971). Other experiments were carried out at the East Rand Proprietary Mine in South Africa (Reines *et al.*, 1965, 1971; Crouch *et al.*, 1978). In these atmospheric neutrino experiments, neutrino events occurring in the rock surrounding a detector were measured. Since the experiments were carried out in extremely deep underground (about 8000 meters water equivalent(m.w.e.)), particles traversing the detectors almost horizontally were almost all of atmospheric neutrino origin. Also, since it was required that the particles should penetrate through the rock (and the detector), most of these events were expected to be charged current (CC) ν_μ interactions.

Another experiment started during the late 1960's (Bergeson, Cassiday and Hendricks, 1973). Since this detector was located at a relatively shallow depth (about 1500 m.w.e.), horizontally-going particles, as well as the downward-going particles, were dominated by cosmic ray muons, and only upward-going muons were selected as neutrino events. 5 events were observed during 603 days of the detector operation.

In the 1970's, the idea of Grand Unified Theories appeared. These theories predicted baryon number non-conservation, i.e., nucleon decay. From the early 1980's, several dedicated proton decay experiments, such as KGF (Krishnaswamy *et al.*, 1981, 1982, 1986), NUSEX (Battistoni *et al.*, 1982, 1983), Soudan-1 (Bartelt *et al.*, 1983), IMB (Bionta *et al.*, 1983; Cortez *et al.*, 1984; Park *et al.*, 1985; Blewitt *et al.*, 1985; Haines *et al.*, 1986; Seidel *et al.*, 1988; Becker-Szendy *et al.*, 1990; McGrew *et al.*, 1999), Kamiokande (Arisaka *et al.*, 1985; Kajita *et al.*, 1986; Hirata *et al.*, 1989), HPW (Phillips *et al.*, 1989), and Frejus (Berger *et al.*, 1989a; 1991a, 1991b) began operation. The background events for the proton decay searches were atmospheric neutrino events. These experiments observed a much larger number of atmospheric neutrino events relative to the previous experiments. Also, these experiments were the first to observe so-called fully-contained events: events for which the neutrinos interact inside the detector and for which all the visible secondary particles stop in the detector. To date, no evidence for nucleon decay has been observed (including results from recent experiments (Allison *et al.*, 1998; Shiozawa *et al.*, 1998; Hayato *et al.*, 1999)). However, these neutrino events were studied carefully by comparing the data and the simulated events to understand the background for the proton decay searches. Various distributions were reported to be reproduced well by the Monte Carlo simulations (Haines *et al.*, 1986; Nakahata *et al.*, 1986). However, IMB-1 (Haines *et al.*, 1986) mentioned that the fraction of events with at least one muon decay was less than expected, 0.26 $\pm$0.03 for the data and 0.34 $\pm$ 0.01 for the Monte Carlo. A similar effect was seen in Kamiokande (Fig.19 of Nakahata *et al.*, 1986).

It was recognized already in the late 1970's (see for example, Bilenky and Pontecorvo, 1978; Pakvasa, 1980; Frampton and Glashow, 1982) that the atmospheric neutrino data can give information on neutrino flavor oscillations, because of the long traveling distance of neutrinos. There were only a few experimental results on neutrino oscillations based on the atmospheric neutrino data in 1980's (Boliev *et al.*, 1981; LoSecco *et al.*, 1985; Bionta *et al.*, 1988). No evidence for neutrino oscillations was observed. (However, we note that the rates of the muon neutrino events observed in Krishnaswamy *et al.* (1971) and Crouch *et al.* (1978) were lower than expected. Although the uncertainty in the predicted flux was large, some authors (for example, Barger *et al.*, 1980; Barger, Whisnant and Phillips, 1980; Pakvasa, 1980) pointed out that these results might suggest that muon neutrinos participate in neutrino oscillations.)

In spite of this progress, interest in atmospheric neutrinos was not very strong until Kamiokande published a study of the atmospheric neutrino data. In 1988, Kamiokande (Hirata *et al.*, 1988) showed a result in which fully-contained single-ring events were separated into muon-(μ-) and electron-(e-)like events. A single-ring μ-like event is produced by a non-showering straight track and is, in most cases, due to either a muon or a pion. A single-ring e-like event is produced by a showering particle and is due to either an electron or a gamma. Kamiokande observed that the number of single-ring μ-like events, which were mostly due to quasi-elastic interactions of atmospheric ν_μ and $\overline{\nu}_\mu$ in the detector, showed a significant deficit compared with the Monte Carlo (MC) prediction, while the number of single-ring e-like events was in good agreement with the expected number. Defining $\mu/e \equiv$(number of μ-like events)/(number

of e-like events), $(\mu/e)_{Data}/(\mu/e)_{MC}$ was $(85/93)/(144.0/88.5) = 0.56^{+0.09}_{-0.08}(stat.)$, where *stat.* means the statistical error. Figure 1 shows, as an example, the momentum distributions of the single-ring e-like and μ-like events in (Hirata *et al.*, 1988). The deficit of μ-like events relative to the MC prediction was significant and did not show any strong momentum dependence. The momentum distribution of e-like events was well explained by the MC prediction.

The prediction of the absolute atmospheric neutrino flux has an uncertainty of $\pm 20\%$. However, the flavor ratio of the atmospheric neutrino flux, $(\nu_\mu + \bar{\nu}_\mu)/(\nu_e + \bar{\nu}_e)$, has been calculated to an accuracy of better than 5% in a broad energy range from 0.1 GeV to higher than 10 GeV. The accurate prediction of this ratio results from the fact that the ν_μ and ν_e are mainly produced by the decay of a pion, $\pi \to \mu\nu_\mu$, and the subsequent decay of the muon, $\mu \to e\nu_e\nu_\mu$, and therefore that the ratio does not depend on the details of the primary cosmic ray flux. The calculated flux ratio has a value of about 2 for energy regions relevant to the Kamiokande data ($E_\nu \sim 1$ GeV). This value is understood because the two muon neutrinos and one electron neutrino produced in the pion's decay chain have approximately the same average energy. Because of the low $(\mu/e)_{Data}/(\mu/e)_{MC}$ ratio, Kamiokande concluded: "We are unable to explain the data as the result of the systematic detector effects or uncertainties in the atmospheric neutrino fluxes. Some as-yet-accounted-for physics such as neutrino oscillations might explain the data." This result triggered interest in atmospheric neutrinos. Some authors (Learned *et al.*, 1988; Barger *et al.*, 1988; Hidaka *et al.*, 1988) analyzed the data in terms of neutrino oscillations.

Soon, thereafter, it was pointed out (Volkova, 1988) that the calculation of the atmospheric neutrino fluxes in (Gaisser *et al.*, 1988), which were used in the analysis of the Kamiokande data, did not take into account the effect of the polarization of cosmic-ray muons in their decay. Muons from pion decay are completely polarized in the pion rest frame. Therefore, the neutrinos from these muons are correlated in angle and energy with the direction of the polarization of the muons. However, none of the flux calculations carried out before 1988 (except for (Volkova, 1980)) took into account this effect. Since neglecting the μ polarization underestimates the energy of ν_e and $\bar{\nu}_e$, the polarization effect accounts for a part of the small μ/e ratio of the data. Following this suggestion, atmospheric neutrino fluxes including this effect were recalculated (Barr *et al.*, 1988; Barr *et al.*, 1989; Honda *et al.*, 1990). It turned out that the change in the $(\nu_\mu + \bar{\nu}_\mu)/(\nu_e + \bar{\nu}_e)$ flux ratio due to the polarization effect was less than 15% at $E_\nu \sim 1$ GeV, which was not large enough to account for the observed ratio. Indeed, the μ/e ratio of the Kamiokande data was still significantly smaller than the prediction based on the calculated fluxes including the polarization effect (Kajita *et al.*, 1990; Hirata *et al.*, 1992).

Following (Hirata *et al.*, 1988), several large underground experiments studied the flavor ratio of atmospheric neutrinos. The observed μ/e ratios by NUSEX (Aglietta *et al.*, 1989) and Frejus (Berger *et al.*, 1989b, 1990) were in agreement with the MC predictions within their statistics. Then, IMB-3 (Casper *et al.*, 1991; Becker-Szendy *et al.*, 1992) published a result on atmospheric neutrinos, showing a smaller μ/e ratio than expected, in good agreement with the Kamiokande result. A μ/e ratio smaller than expected was also observed recently by the Soudan-2 experiment (Allison *et al.*, 1997, 1999).

Neutrino oscillations were suggested to explain the small μ/e ratios. For detectors near the surface of the Earth, the neutrino flight distance, and thus the oscillation probability, varies as a function of the zenith angle of the neutrino direction. Vertically downward-going neutrinos travel about 15 km while vertically upward-going neutrinos travel about 13,000 km before interacting in the detector. The broad energy spectrum from a few hundred MeV to about 100 GeV and the broad range of neutrino flight distances make measurements of atmospheric neutrinos sensitive to neutrino oscillations for Δm^2 down to 10^{-4} eV^2.

For neutrino energies higher than a few GeV, the fluxes of upward and downward going neutrinos are expected to be nearly equal: the geomagnetic field effects on atmospheric neutrinos in this energy range are expected to be small because the primary cosmic rays that produce these neutrinos have rigidities ($\equiv$ momentum/charge) exceeding the geomagnetic cutoff rigidity ($\sim$10 GeV/Ze). A zenith angle dependence of the neutrino fluxes at high energies was measured by the Kamiokande experiment (Fukuda *et al.*, 1994). The observed zenith angle-dependent deficit of μ-like events, together with the small μ/e ratio, strongly suggested neutrino oscillations. However, the observed deficit of upward-going μ-like events relative to the downward going ones in the high energy regions was only a 2.9 standard deviation effect and was not conclusive. Based on these measurements, Kamiokande estimated the allowed parameter regions of neutrino oscillations (Hirata *et al.*, 1992; Fukuda *et al.*, 1994). Because of the relatively small statistics, discrimination between $\nu_\mu \to \nu_e$ and $\nu_\mu \to \nu_\tau$ oscillations was not possible and both possibilities were allowed.

Recently, long baseline reactor experiments, CHOOZ (Apollonio *et al.*, 1998, 1999) and Palo Verde (Boehm *et al.*, 2000), did not observe any evidence for $\bar{\nu}_e \to \bar{\nu}_x$ oscillations, and ruled out the $\nu_\mu \to \nu_e$ solution of the atmospheric neutrino problem.

The upward-going muons observed in underground detectors are the products of neutrino interactions in the rock. The mean neutrino energy of these events is of the order of 100(10) GeV for through-going(stopping) events. These

events are used for an independent check of the neutrino oscillation analysis of the lower energy atmospheric neutrino data.

Super-Kamiokande, a 50,000 ton water Cherenkov detector started taking data in 1996. In 1998, this experiment, with approximately a factor of four more fully-contained and partially-contained events than the Kamiokande data, together with the analysis of upward-going muons, concluded that the atmospheric neutrino data gave evidence for neutrino oscillations.

In the following sections, details of the atmospheric neutrino observations are described. Section II describes calculations of the atmospheric neutrino fluxes. Section III outlines the simulation of neutrino interactions relevant to the energy range of atmospheric neutrinos. Sections IV and V describe the details of the atmospheric neutrino data and the neutrino oscillation analyses. Then, in Section VI, various attempts to explain the atmospheric neutrino data by other physics are briefly described. Section VII summarizes this article. In this article, when mention is made of neutrinos, we imply both neutrinos and anti-neutrinos.

II. FLUX CALCULATION

Atmospheric neutrino fluxes have been calculated by many authors (for example, Lipari, Stanev and Gaisser, 1998; Agrawal *et al.*, 1996; Honda *et al.*, 1990, 1995; Perkins, 1994; Lipari, 1993; Bugaev and Naumov, 1989; Lee and Koh, 1990; Butkevich, Dedenko and Zheleznykh, 1989; Barr, Gaisser and Stanev, 1989; Gaisser *et al.*, 1983; Dar, 1983; Volkova, 1980; Tam and Young, 1969; Osborne, Said and Wolfendale, 1965). The difficulties and the uncertainties in the calculation of atmospheric neutrino fluxes differ for high and low energies. Low energy neutrinos with energies near 1 GeV are mostly produced by primary cosmic rays with energies of less than 100 GeV. In this energy range, the primary cosmic ray fluxes are modulated by solar activity. Also, the cosmic ray fluxes at the top of the atmosphere are affected by the geomagnetic field through the rigidity ($\equiv$ momentum/charge) cutoff. These effects must be carefully taken into account in the flux calculation. High energy neutrinos with energies near 100 GeV are mainly produced by primary cosmic rays with energies near 1000 GeV or higher. In this energy range, the solar activity and the rigidity cutoff do not affect the cosmic rays. However, in the high energy range, details of the primary cosmic ray fluxes have not been measured, and therefore the accuracy of the absolute flux calculation is limited.

In this article, we outline the methods and results of flux calculations for the two most detailed calculations (Lipari, Stanev and Gaisser, 1998, Agrawal *et al.*, 1996, and Honda *et al.*, 1990, 1995). These fluxes are used for analyses of recent atmospheric neutrino data. In these calculations, Monte Carlo methods are used to include accurately various effects relevant to the calculations. For other methods and results, see the original reports.

In the flux calculations, a one-dimensional approximation is used, i.e., after the interaction of primary cosmic ray particles with air nuclei, all the particles are assumed to be moving along the line of the momentum vector of the primary cosmic ray particle. Recently, preliminary results of three-dimensional flux calculations have been reported (Battistoni *et al.*, 2000; Tserkovnyak *et al.*, 1999; Lipari, 2000a). However, in this article, we use the fluxes calculated by the one-dimensional approximation, because (a) the new fluxes based on the three-dimensional calculations have not yet been used in the Monte Carlo calculations of the atmospheric neutrino experiments, and (b) the expected energy and angular distributions of the produced leptons based on the three-dimensional calculation are similar to those based on the one-dimensional calculation.

A. Flux of primary cosmic rays

Primary cosmic ray fluxes have been measured by many experiments. In the energy range below about 100 GeV, the most accurate flux measurements were carried out by magnetic spectrometers with particle identification devices. Between 1000 and 10^5 GeV, the energies and the fluxes of the cosmic ray particles were measured by calorimeter and emulsion chamber techniques.

The fluxes of cosmic ray particles heavier than a proton have also been measured. For example, from the compilation of Webber and Lezniak (1974), the composition of cosmic rays is H$\sim$95%, He$\sim$4.5% and CNO (plus heavier nuclei) $\sim$0.3% above 2 GeV/nucleus. We note that the neutrino fluxes are dependent on the number of nucleons rather than the number of nuclei. Helium nuclei carry about 15% of the total nucleons in the cosmic ray flux and the CNO (plus the heavier) group carries about 3.6% above 2 GeV/nucleon. Therefore we roughly expect that about 20% of the total neutrino flux is produced by He and CNO primaries. Figure 2 shows the measured energy spectrum of primary cosmic ray fluxes. Since the energy spectrum of the cosmic rays is very soft (the flux is roughly proportional to $E^{-2.7}$ above 10 GeV), the fluxes are multiplied by a factor of $E^{2.75}$ in this figure. The fluxes used in the neutrino flux calculations

are also shown. The proton flux assumed in (Honda *et al.*, 1995) is higher than that in (Agrawal *et al.*, 1996) in the energy range between 10 and 10000 GeV by at most 30%. We comment that the more recent proton flux data below 100 GeV favors the low flux in Figure 2 (top), and therefore the proton flux used in (Honda *et al.*, 1995) is likely to be overestimated at around 100 GeV proton energy.

B. Solar modulation

The flux of low energy cosmic rays is modulated by solar activity. The strength of the solar wind (an outflow of plasma from the Sun), which is correlated with the solar activity, varies with an 11 year period. The magnetic field associated with the solar wind drives back the low energy cosmic rays which are entering into the solar sphere. This effect increases as cosmic ray energy decreases. The flux difference at solar maximum and solar minimum is more than a factor of 2 for 1 GeV cosmic ray protons and is about 10~20% for 10 GeV cosmic ray protons. However, this variation has a relatively small effect on the calculation of atmospheric neutrino fluxes, because the geomagnetic field prevents these low energy cosmic-ray particles from entering into the atmosphere anyway (see below).

C. Geomagnetic field and rigidity cutoff

The geomagnetic field bends the trajectory of cosmic ray particles, and therefore determines the minimum rigidity at which a cosmic ray can arrive at the Earth (cutoff rigidity). The cutoff rigidity is a function of the entering position on the Earth and the arrival direction.

The geomagnetic field can be represented by a multi-pole expansion of the spherical harmonic function (Honda *et al.*, 1990). Then the value of the cutoff rigidity for a position on the Earth and for a particle direction is obtained by computer modeling of cosmic ray trajectories. In the simulation, an antiproton is used as a test particle. To estimate the cutoff rigidity at different positions and for different directions, test particles are launched from the surface of the Earth, varying the position and the direction. When a test particle with a given energy and direction escapes to infinity, it is concluded that a cosmic ray with the same energy and mass and the opposite direction and charge can enter into the atmosphere and reach the same position on the Earth. Figure 3 illustrates typical allowed and forbidden tracks of cosmic rays. The cutoff rigidity is calculated as the minimum rigidity with which the test particle escapes from the geomagnetic field. The cutoff rigidity at Kamioka calculated in this way (Honda *et al.*, 1995) is shown in Figure 4. (We note, however, that the exact definition of the cutoff rigidity is more complicated. For a full discussion of the cutoff rigidity, see for example (Hillas, 1972).)

D. Interaction of cosmic rays in the air

As cosmic ray particles propagate in the atmosphere, they interact with air nuclei, producing π and less abundantly K mesons. The mesons and muons produced by these meson decays produce atmospheric neutrinos when they decay. In the simulation of cosmic ray interactions with air nuclei, different models were used in Honda *et al.* (1995) and Agrawal *et al.* (1996). Agrawal *et al.* (1996) developed their own interaction model, TARGET (Gaisser, Protheroe and Stanev, 1983). On the other hand, the interaction model used in Honda *et al.* (1995) is composed of three different models: NUCRIN (Hänssget and Ranft, 1986) for particle energy of less than 5 GeV, LUND code, FRITIOF ver.1.6 (Nilsson-Almqvist and Stenlund, 1987) and JETSET ver.6.3 (Sjöstrand and Bengtsson, 1987) for 5 to 500 GeV, and an air-shower simulation program, COSMOS (Kasahara *et al.*, 1979), for energies higher than 500 GeV.

There are uncertainties in the charged pion multiplicity from cosmic ray interactions with air nuclei. Also, the uncertainties in the pion momentum spectrum have non-negligible effects on the calculation of the flux of atmospheric neutrinos. Gaisser *et al.* (1996) compared the pion multiplicity and momentum distributions for various flux calculations. The pion momentum spectrum of Honda *et al.* (1995) was softer than that of Agrawal *et al.* (1996). As we will show later in Figure 6, the calculated flux values in Honda *et al.* (1995) and Agrawal *et al.* (1996) agree within 10% in the energy range of around 1 GeV due to a partial cancellation of the softer pion spectrum and the higher primary cosmic ray fluxes of Honda *et al.* (1995) compared with those of Agrawal *et al.* (1996). However, the agreement at this level is likely to be accidental.

Finally, we comment that the proper modeling of the density structure of the atmosphere is important, because this structure partly determines the zenith angle dependence of the neutrino flux.

E. Calculated flux of atmospheric neutrinos

In this section, the results from the most detailed calculations of the atmospheric neutrino fluxes are presented. Since the fluxes in the low energy region depend on the location on the Earth, we show the fluxes calculated at Kamioka in Japan.

The calculated energy spectra of atmospheric neutrinos are shown in Figure 5. Also shown in Figure 6 is the comparison of the calculated fluxes as a function of neutrino energy. The calculated fluxes by Honda *et al.* (1995) and Agrawal *et al.* (1996) agree at the 10% level. However, we note that the systematic error in the calculated absolute flux values should be larger than 10%, because the primary cosmic ray flux measurements have relatively large uncertainties in their absolute normalization. These authors estimate that the systematic uncertainty of the absolute flux value is about 20%.

An important check of the absolute flux value can be made by comparing the observed and calculated fluxes of atmospheric muons. Since the muons appear in the middle of the $\pi \to \mu\nu_\mu$, $\mu \to e\nu_e\nu_\mu$ decay chain, the energy spectra of these muons and neutrinos are well correlated. Figure 7 shows the comparison of the observed and calculated muon fluxes at various atmospheric heights (Honda *et al.*, 1995). The observed and calculated fluxes agree reasonably well except for those at very high altitude ($\gtrsim 37\ g/cm^2$). We note that the good agreement of the absolute neutrino fluxes calculated in Honda *et al.* (1995) and Agrawal *et al.* (1996) could be in part due to the fact that they both compare their calculated muon fluxes to the common atmospheric muon data.

Figure 8 shows the calculated $(\nu_\mu + \overline{\nu}_\mu)/(\nu_e + \overline{\nu}_e)$ flux ratio as a function of neutrino energy integrated over the solid angle. The calculated flux ratio is about 2 for neutrino energies less than a few GeV. This ratio results from the fact that a π-decay produces a ν_μ and a μ: the μ, when it decays, produces another ν_μ and a ν_e. Furthermore, the three neutrinos produced in the pion's decay chain have approximately the same average energy. The flux ratio increases with increasing neutrino energy. This increase results from the fact that the probability of a muon surviving to reach the ground increases with increasing muon energy. As expected, the two calculated ratios agree within 5% in the energy range between 0.1 and 30 GeV. This ratio is essentially independent of the primary cosmic ray spectrum. In the energy region of less than about 10 GeV, where most of the neutrinos are produced by the decay chain of pions, the expected uncertainty of this ratio is less than 5%. In the higher energy region ($\gtrsim$30 GeV), the contribution of K decay in the neutrino production is more important. Therefore the ratio depends more on the K production cross sections and the uncertainty of the ratio is expected to be larger.

Figure 9 shows the calculated $\nu_\mu/\overline{\nu}_\mu$ and $\nu_e/\overline{\nu}_e$ flux ratios as a function of neutrino energy integrated over the solid angle. The agreements between the calculations are at about the 5% level for both the $\nu_\mu/\overline{\nu}_\mu$ ($E_\nu \lesssim 10\ GeV$) and $\nu_e/\overline{\nu}_e$ flux ratios. It is clearly seen that the $\nu_\mu/\overline{\nu}_\mu$ ratio in the low-energy region is near unity. This can be understood because each of the π^+ and π^- decay chains produce one ν_μ and one $\overline{\nu}_\mu$ at low energies where most of the muons decay before reaching to the ground. Therefore, the $\nu_\mu/\overline{\nu}_\mu$ ratio does not depend on the details of the π^+/π^- production ratio in the interactions of the primary cosmic rays with air nuclei. In contrast, the $\nu_e/\overline{\nu}_e$ ratio at low energy is slightly larger than unity, reflecting the π^+/π^- production ratio, because a $\pi^+(\pi^-)$ produces a $\nu_e(\overline{\nu}_e)$ through the $\pi \to \mu \to e$ decay chain.

Figure 10 shows the zenith angle dependence of the atmospheric neutrino fluxes for several neutrino energies. The fluxes of the downward-going neutrinos are lower than those of the upward-going neutrinos at low energies. This is due to the geomagnetic field effect (cutoff rigidity): i.e., the cutoff rigidity near Kamioka is higher than the averaged cutoff rigidity over the Earth. (The map of the cutoff rigidity at the Kamioka site is shown in Figure 4. Clearly, the averaged cutoff rigidity for down-going directions is higher than that for up-going directions.) However, for neutrino energies of higher than a few GeV, the calculated fluxes are essentially up-down symmetric, because the geomagnetic field effect is negligible in the high energy regions.

The flight length of neutrinos is an important input to the analysis of neutrino oscillations. For neutrinos passing through the Earth, the flight length can be easily calculated. However, for neutrinos produced in the upper atmosphere, the flight-length distribution must be calculated by a Monte Carlo method (Honda *et al.*, 1995; Gaisser and Stanev, 1998). Figure 11 shows the distribution of calculated flight length of neutrinos for vertically downward-going directions. The mean flight length for these neutrinos is about 15 km. Figure 12 shows the calculated mean flight length of neutrinos as a function of the zenith angle for three neutrino energies. Since electron neutrinos (muon neutrinos) are mainly produced by muon decays (pion and muon decays), and since the muon lifetime is much longer than the pion lifetime, there is a stronger energy dependence in the flight length for the downward-going electron neutrinos than for the muon neutrinos.

In summary, we remark that, while the absolute flux value has an uncertainty of about 20%, the $(\nu_\mu + \overline{\nu}_\mu)/(\nu_e + \overline{\nu}_e)$ flux ratio is predicted to an accuracy of better than 5% and the zenith angle dependence of the flux is well understood.

In particular, above a few GeV neutrino energies, the flux is predicted to be essentially up-down symmetric.

III. SIMULATION OF THE ATMOSPHERIC NEUTRINO INTERACTIONS

A. Neutrino interactions

The important energy range for contained neutrino interactions is between 0.1 and 100 GeV. To understand the details of atmospheric neutrino events, each experiment has developed its own Monte Carlo simulation.

As an example, in the Monte Carlo simulation of the Super-Kamiokande experiment, the following 8 types of reactions were simulated:

1. Charged-current quasi-elastic interaction; $\nu(\overline{\nu})N \rightarrow l^{\pm}N'$.
2. Charged-current single-pion production through baryon resonances; $\nu(\overline{\nu})N \rightarrow l^{\pm}\pi N'$.
3. Charged-current coherent pion production; $\nu(\overline{\nu})O \rightarrow l^{\pm}\pi^{\mp}O$.
4. Charged-current multi-hadron production; $\nu(\overline{\nu})N \rightarrow l^{\pm}(m\pi)N'$ $(m \geq 1)$.
5. Neutral-current elastic interaction; $\nu(\overline{\nu})N \rightarrow \nu(\overline{\nu})N'$.
6. Neutral-current single-pion production through baryon resonances; $\nu(\overline{\nu})N \rightarrow \nu(\overline{\nu})\pi N'$.
7. Neutral-current coherent pion production; $\nu(\overline{\nu})O \rightarrow \nu(\overline{\nu})\pi^0 O$.
8. Neutral-current multi-hadron production; $\nu(\overline{\nu})N \rightarrow \nu(\overline{\nu})(m\pi)N'$ $(m \geq 1)$.

$l^{\pm}$, $N(N')$ and O represent a charged lepton, a nucleon and an oxygen nucleus, respectively. In the lowest energy region of $E_\nu \lesssim 0.5$ GeV, the quasi-elastic interaction is the dominant interaction. Near 1 GeV, the single-pion production is also important. In the higher energy region, the multi-hadron production processes by deep inelastic scattering are dominant.

The models by Llewellyn Smith (1972), Rein and Sehgal (1981), Rein and Sehgal (1983), and the deep-inelastic interaction formulae with structure functions from GRV94 (Glück, Reya, and Vogt, 1995) were used for the simulation of the (quasi-) elastic interactions, the single-pion production through baryon resonances, the coherent pion production and the multi-hadron production, respectively. The momentum spectrum of the particles (most of them are pions) produced by these deep-inelastic neutrino interactions were simulated based on JETSET 7.4 (Sjöstrand, 1994).

The actual neutrino interactions with a nucleus (H_2O, Fe) are more complicated than those with a free nucleon, because nucleons in a nucleus are bound. For nucleons bound in a nucleus, the Fermi motion of the target nucleon must be taken into account. For (quasi-) elastic interactions, the Pauli exclusion principle must also be taken into account. The actual treatment of these effects was made using the Fermi-gas model, in such a way that the momentum of the recoil nucleon must exceed the Fermi surface momentum (taken to be 217 MeV/c).

The total cross section was taken to be the sum of the cross section of each channel. Figure 13 shows the CC total cross section as a function of neutrino energy. The simulation reproduces the cross section data within $\pm 15\%$.

Finally, we comment that the threshold energy of CC ν_τ interaction is about 3.5 GeV and that the CC cross section of ν_τ is significantly smaller than that of ν_μ even above the threshold, due to the heavy tau mass. Figure 14 shows the calculated total cross section ratio of $\nu_\tau N$ and $\nu_\mu N$ interactions.

B. Pion interactions

Pions produced by a neutrino interaction in a nucleus often undergo secondary nuclear interactions before leaving the nucleus. This effect was taken into account in the Monte Carlo simulation of Super-Kamiokande based on the model of Oset *et al.* (1988). Figure 15 shows the probability of various nuclear interactions of π^0 generated randomly in a ^{16}O nucleus before leaving the same nucleus. It is clear that the nuclear effect on pions is relatively large. Due to this effect, a fraction of CC single-pion production events have no pion emerging from the nucleus. This effect is important, since, for example, Super-Kamiokande uses mostly single-ring events for the neutrino oscillation analysis.

Charged pions which propagate in the detector material undergo nuclear interactions. In the Super-Kamiokande Monte Carlo simulation, this effect was simulated based on the CALOR model (Gabriel *et al.*, 1989) in the energy range above 500 MeV. In the energy range below 500 MeV, a specially developed simulation program was used (Nakahata *et al.*, 1986). The reproducibility of these simulation programs was studied in a beam test using a 1 kton water Cherenkov detector at KEK (Kasuga *et al.*, 1996).

IV. ATMOSPHERIC NEUTRINO EXPERIMENTS

A. General remarks

The rate of atmospheric neutrino interactions is about 0.5 per kton per day. Since the background rate at the surface due to cosmic ray particles is so large, $\sim 2 \times 10^2/\mathrm{m}^2/\mathrm{sec}$, it is unrealistic to carry out atmospheric neutrino experiments at the surface with present technology. Hadrons, electrons and gammas from cosmic ray showers, which are still remaining at the surface, are quickly absorbed by several meters of rock. Muons, which make up a large fraction of the secondary cosmic rays at the surface, lose their energy mainly by ionization and penetrate deeper into the earth. The muons at the surface have a mean energy of about 2 GeV and a differential energy spectrum falling as E_μ^{-2} at $E_\mu = 10$ GeV, steepening smoothly to $E_\mu^{-3.6}$ above 1 TeV (Allkofer, Carstensen and Dau, 1971). In order to reduce the atmospheric muon flux significantly, the detector must be located deep underground. Figure 16 shows the depth of the detectors and the cosmic ray muon rate. Even at a depth of 2700 m.w.e. (meters water equivalent, 1000 m underground for standard rock), Super-Kamiokande observes about 2 muons per second. This rate should be compared with the observed atmospheric neutrino rate in the fiducial volume of the same detector - about 9 events per day. The rate of muons is $\sim 2 \times 10^4$ times higher than the rate of atmospheric neutrino events in Super-Kamiokande.

B. Detectors

The present atmospheric neutrino detectors can be classified into three types. One type comprises gas-counter, iron-plate tracking calorimeters, which detect the tracks of charged particles. Examples of this type of detector are Frejus (Berger *et al.*, 1987), NUSEX (Battistoni *et al.*, 1986), and Soudan-2 (Allison *et al.*, 1996a, 1996b). These detectors record a three-dimensional view of events with about 1 cm segmentation size, and detailed studies of complicated events are possible. In these detectors, fully-contained and partially-contained events have been observed. However, upward-going muons, which are produced by high energy ν_μ interactions below the detector, have not been identified due to the lack of the fast timing and the resulting ambiguity between upward- and downward-going muons.

The second type comprises imaging water Cherenkov detectors. Examples are Kamiokande (Nakamura *et al.*, 1994), IMB-3 (Becker-Szendy *et al.*, 1993, 1994) and Super-Kamiokande (Fukuda *et al.*, 1998a). As an example, Figure 17 shows the Super-Kamiokande detector. Since Photo-Multiplier-Tubes (PMTs) placed at the surface of a detector are used to detect Cherenkov photons, it is possible to construct relatively large detectors for a limited cost. On the other hand, since the three-dimensional topology of an event must be reconstructed from the information recorded on the detector surface, generally the reconstruction program is not simple. However, for events with a single Cherenkov ring, the accuracy of various quantities such as the energy resolution and particle identification is even better than those of tracking calorimeters. Three types of events – fully-contained, partially-contained and upward-going muon events – have been observed in water Cherenkov detectors.

The third type of atmospheric neutrino detector comprises liquid scintillator detectors (combined with some tracking devices). Examples are Baksan (Boliev *et al.*, 1991) and MACRO (Ahlen *et al.*, 1993). Taking advantage of good timing resolution, these detectors can observe upward-going muons. Table I summarizes the main features of atmospheric neutrino experiments.

V. OBSERVATION OF ATMOSPHERIC NEUTRINOS AND NEUTRINO OSCILLATIONS

Atmospheric neutrino events are usually categorized into four types: fully-contained (FC) events, partially-contained events (PC), upward stopping muon events and upward through-going muon events. FC events have their vertex positions in the fiducial volume of the detector and have all the visible secondary particles stopping in the detector. PC events have their vertex positions in the fiducial volume and have at least one charged track exiting the detector. Most PC events are CC ν_μ events, since a particle must propagate in the detector material for a relatively long distance to satisfy the requirement of partial containment. Upward-going muon events are neutrino interactions occurring in the rock surrounding the detector. Only muons are observed, since the electrons, photons and hadrons are absorbed by a few meters of rock. Almost all upward-going muon events are due to CC ν_μ interactions. The estimated fractions of CC ν_e, CC ν_μ and neutral current (NC) interactions for each event type are summarized in Table II based on the Super-Kamiokande Monte Carlo and analysis. The estimated neutrino energies for various types of atmospheric neutrino events are shown in Figure 18. Typical neutrino energies of FC, PC, upward stopping muon and upward

through-going muon events are of the order of 1, 10, 10 and 100 GeV, respectively. In this section, FC and PC events are described first. Then upward-going muon events are described.

A. Contained neutrino events

1. Selection of atmospheric neutrino events

In very deep underground experiments such as Frejus (Berger *et al.*, 1989b) and NUSEX (Aglietta *et al.*, 1989), the trigger rates were very low, about 7 and 45 events per hour for NUSEX and Frejus, respectively. Atmospheric neutrino events were selected by requiring the primary vertex in the fiducial volume. In NUSEX, only fully-contained (FC) events were used for the analysis. In Frejus, both FC and partially-contained (PC) events were used in the analysis.

Some of the detectors located at less deep places (Kamiokande (Fukuda *et al.*, 1994), Soudan-2 (Allison *et al.*, 1999), and Super-Kamiokande (Fukuda *et al.*, 1998a, 1998b)), consisted of an outer anti-counter and an inner detector. In Kamiokande and Super-Kamiokande, most of the cosmic ray muons were rejected by requiring no signal in the anti-counter. For example, in Super-Kamiokande, after the software reduction which essentially required no anti-counter signal, about 20 events per day survived. These events were then doubly scanned by physicists. After the scanning, about 5 events per day were rejected as background events. Most of the background events were "flashing PMT" events (events caused by light emitted by internal corona discharges of one of the PMTs).

In Soudan-2, a different approach was taken. Events with reconstructed vertices in the fiducial volume were selected without using any anti-counter information. Then the events were classified into "gold" and "rock" events according to the anti-counter information. "Gold" events have no anti-counter hit signal and should be primarily neutrino events. The "rock" events have anti-counter hits and are background events. Since there could be some contamination of background events among the "gold" events, the distribution of the minimum distance between the event vertex and the detector exterior (excluding the detector floor) was studied. Generally, the vertex positions of the background events should cluster near the exterior of the detector. The distributions are shown in Figure 19. About 80% of the "gold" events were fitted as neutrino events, and were used for further analyses. In Soudan-2, to date, only analyses of FC events have been published.

In IMB-3 (Becker-Szendy *et al.*, 1992), there were 10^4 triggers per hour. Most of them were cosmic ray muons. About 10 events per day survived software cuts. These events were then scanned by physicists, and any events confirmed to originate inside the fiducial volume were saved as atmospheric neutrinos.

In Kamiokande and Super-Kamiokande, PC events were systematically studied. The selection of PC events required special criteria (Fukuda *et al.*, 1994, 1998b), because these events had anti-counter signals. Super-Kamiokande reduced the number of PC event candidates to about 2 events per day by software cuts. Then finally, these events were scanned, and the final PC event sample was made. The rate of the PC events at this stage (before the fiducial volume cut) was about 0.8 events per day.

The numbers of the observed events and the detector exposures from each experiment are summarized in Table I.

2. General distributions

Before discussing the data related to neutrino oscillations, we briefly discuss distributions which are relatively insensitive to neutrino oscillations.

The vertex positions of atmospheric neutrino interactions must be distributed uniformly within the detector. On the other hand, the vertex positions of background events should be clustered near the surface of the detector. The distribution of vertex positions is therefore useful to check the background contamination. Figure 20 shows the distance of the reconstructed vertex position from the PMT plane of the inner detector of Super-Kamiokande (D_{wall}) for the FC events. The observed event rate was lower than that for the Monte Carlo prediction. However, the observed event rate was also consistent with the prediction within the uncertainty in the absolute neutrino flux. Some excess of events near $D_{wall} = 0$ was seen. However, this excess was not seen for events with $D_{wall} > 0.5$ m. Therefore, within the fiducial volume of D_{wall} >2 m, there was no evidence for contamination from non-neutrino background.

A similar study was carried out by the Soudan-2 experiment. As previously shown in Figure 19, the background contamination in the FC sample was estimated using the vertex position distribution of the background events with the anti-counter hits. The background contamination in the Soudan-2 FC sample was estimated to be about 20%. The larger background contamination in Soudan-2 than in Super-Kamiokande can be understood to be due to the

shallower detector position and the thinner detector region outside of the fiducial volume in Soudan-2. In Soudan-2, the fiducial volume is defined to be 20 cm from the surface of the detector. The average density of the detector is 1.6 g/cm^3. In Super-Kamiokande, the thickness of the water from the surface of the detector to the surface of the fiducial volume is 4.6 to 4.75 m, which is thick enough to eliminate most of the gamma-ray and neutron background events.

Figure 21 shows the visible energy (E_{vis}) distribution of FC events observed in Super-Kamiokande. The shape of this distribution was in reasonable agreement with the corresponding Monte Carlo prediction over a wide energy range from 100 MeV to 100 GeV.

Figure 22 (a) shows the distribution of the number of the observed charged tracks per event in the Frejus experiment. Figures 22 (b) and (c) show the distributions of the number of Cherenkov rings in the Kamiokande and Super-Kamiokande experiments, respectively. In these figures, the shapes of the distributions of the data were in reasonable agreement with the corresponding simulations. In summary, the Monte Carlo simulations of atmospheric neutrino interactions reasonably reproduced these global distributions of the data.

3. Flux ratio

The atmospheric (ν_μ/ν_e) flux ratio has been measured by identifying electrons and muons produced by CC ν_e and CC ν_μ interactions, respectively. Electrons produce electromagnetic showers while propagating in matter. On the other hand, muons slowly lose their energy by dE/dx while propagating in matter. The different propagation of these particles in matter is used to separate electrons and muons. The efficiency for separating CC ν_e and ν_μ events (or e-like and μ-like events), i.e., the probability that an electron(muon) track is identified as 'e' ('μ'), is generally high in the present atmospheric neutrino experiments: 85$\sim$99% depending on the experiment.

In tracking calorimeters, the event pattern is recorded in a 3-dimensional view, and the separation of electrons and muons is carried out by event pattern recognition. Figure 23 shows examples of events observed by the Soudan-2 detector. CC ν_μ events are clearly recognized by a (long) straight track, which is a candidate muon. A CC ν_e event, on the other hand, has an electromagnetic shower linked to the vertex point.

In water Cherenkov detectors, CC ν_e and ν_μ events are distinguished by the difference of the characteristic shape of the Cherenkov ring. Figure 24 shows examples of (a) an e-like and (b) a μ-like event observed in the Super-Kamiokande detector. A clear outer edge of the Cherenkov light is identified for a μ-like event, while the edge is relatively unclear for an e-like event due to an electromagnetic shower and the multiple scattering of low-energy electrons. The particle identification techniques of the Kamiokande experiment (Kasuga *et al.*, 1996) (which was used in the Super-Kamiokande experiment with some improvements) and the IMB-3 experiment (Breault, 1997) were tested using a beam at KEK. In water Cherenkov detectors, most analyses are carried out using the single Cherenkov ring events to minimize the systematic errors related to the use of multi-ring events. In tracking calorimeters, multi-prong events are also used based on suitable criteria to select lepton candidates.

Based on the particle identification technique, the flavor ratio in the atmospheric neutrino flux was measured. The $(\nu_\mu+\overline{\nu}_\mu)/(\nu_e+\overline{\nu}_e)$ flux ratio has been calculated to an accuracy of better than 5%, and therefore the measurement of this ratio is sensitive to neutrino oscillations. Experimentally, the μ-like/e-like ratio for the data is compared with the same ratio for the MC. Therefore, $(\mu\text{-like}/e\text{-like})_{Data}/(\mu\text{-like}/e\text{-like})_{MC}$ should be consistent with unity within the experimental errors for the case of no neutrino oscillations. Figure 25 summarizes the $(\mu/e)_{Data}/(\mu/e)_{MC}$ measurements from various experiments. Measurements from Kamiokande (both sub- and multi-GeV data samples), IMB-3 (sub-GeV), Soudan-2 and Super-Kamiokande (both sub- and multi-GeV data samples) showed $(\mu/e)_{Data}/(\mu/e)_{MC}$ ratios which were smaller than unity. The sub-GeV(multi-GeV) sample in Kamiokande and Super-Kamiokande was defined to included events with E_{vis} <1.33 (>1.33) GeV. E_{vis} =1.33 GeV corresponds to an electron(muon) momentum of 1.33 (about 1.4) GeV/c. The statistical errors from these measurements, especially those from Super-Kamiokande, were so small that statistical fluctuations cannot explain the smallness of these measurements. There were a few measurements suggesting a ratio consistent with unity. However these measurements had relatively large statistical errors.

Since many of the uncertainties of the prediction and the experiment cancel when taking this ratio, the systematic error of this measurement was relatively small. As an example, we summarize, in Table III, the sources of the systematic error in the Super-Kamiokande analysis. Among them, the largest contribution came from the uncertainty in the calculated (ν_μ/ν_e) flux ratio in the sub-GeV energy range, and from the single-ring and multi-ring separation uncertainty in the multi-GeV energy range. Neither a statistical fluctuation nor systematic uncertainties can explain the small (μ/e) ratio of the data.

4. Momentum distribution

The momentum spectra of e-like events and μ-like events from Super-Kamiokande are shown in Figure 26. The shapes of the observed momentum spectra agreed well with the MC predictions. Figure 27 compares the momentum dependence of $(\mu/e)_{Data}/(\mu/e)_{MC}$ from various experiments. Data from these experiments agreed reasonably well. No strong momentum dependence was seen in $(\mu/e)_{Data}/(\mu/e)_{MC}$.

5. Zenith angle distribution

The flight length of the atmospheric neutrinos varies from ~15 km to 13000 km depending on the zenith angle of the neutrino direction (see Figure 12). Therefore, if the observed small $(\mu/e)_{Data}/(\mu/e)_{MC}$ ratio is due to neutrino oscillations and if the oscillation length is between ~15 km and 13000 km, it should be possible to observe a zenith angle-dependent deficit (and possibly excess) of the neutrino flux. However, the direction of the neutrino must be estimated from the reconstructed direction of the products of the neutrino interaction. In water Cherenkov detectors, the direction of an observed charged lepton is assumed to be the direction of the neutrino. Figure 28 shows the estimated correlation angle between the neutrinos and the leptons as a function of the lepton momentum. At energies below ~400 MeV/c, the lepton direction has little correlation with the neutrino direction. The correlation angle becomes smaller with increasing lepton momentum. Therefore, the zenith angle dependence of the flux as a consequence of neutrino oscillations is largely washed out below 400 MeV/c lepton momentum. With increasing momentum, the effect can be seen more clearly.

The zenith angle distributions of e-like and μ-like events from Super-Kamiokande and Kamiokande are shown in Figures 29 and 30, respectively. The μ-like data, especially in the multi-GeV energy region from Super-Kamiokande, exhibited a strong up-down asymmetry in zenith angle (Θ) while no significant asymmetry was observed in the e-like data. The zenith angle distributions of the Kamiokande data agreed reasonably with those of Super-Kamiokande. However the zenith angle distribution of the Kamiokande sub-GeV μ-like events did not show any significant up-down asymmetry. For further analyses, we define the up-down double-ratio, $(U/D)_{Data}/(U/D)_{MC}$, where U is the number of upward-going events ($-1 < \cos\Theta < -0.2$) and D is the number of downward-going events ($0.2 < \cos\Theta < 1$). This ratio is expected to be consistent with unity within errors for no neutrino oscillations. For the multi-GeV FC+PC μ-like events from Super-Kamiokande, shown in Figure 29, the $(U/D)_{Data}/(U/D)_{MC}$ value was $0.54 \pm 0.04(stat.) \pm 0.01(syst.)$, where *syst.* means the systematic error. It deviated from unity by 8 standard deviations. The Kamiokande $(U/D)_{Data}/(U/D)_{MC}$ value for the multi-GeV FC+PC μ-like events, shown in Figure 30, was $0.59\ ^{+0.13}_{-0.11}(stat.)$. These measurements agreed well. These measurements, which were close to 0.5, suggest a near-maximal neutrino mixing, since $(U/D)_{Data}/(U/D)_{MC} \simeq 1 - (\sin^2 2\theta)/2$ to first approximation, assuming that there is no (full) oscillation effect for downward-(upward-) going particles, and averaging over the energy spectrum.

In tracking calorimeters, especially in Soudan-2, it is possible to identify protons recoiled from the neutrino interactions. For events with an identified lepton plus a proton in the final state, the neutrino direction can be determined accurately. However, the actual resolution of the neutrino direction is limited for reasons including: Fermi motion of the target nucleons, nuclear effects on the recoil protons, and a contamination of single-pion production events with the pions being absorbed in the target nucleus. Soudan-2 studied the zenith angle distribution by selecting quasi-elastic-like events with the following criteria: (a) a recoil proton should be observed and the lepton momentum should be higher than 150 MeV/c, or (b) the lepton momentum should be higher than 600 MeV/c if the recoil proton was not identified. In addition, multi-prong events with $E_{vis} > 700$ MeV, total momentum > 450 MeV/c and lepton momentum > 250 MeV/c were used. The estimated resolutions of the neutrino direction reconstruction were 21 and 33 degrees for the CC ν_e and CC ν_μ samples, respectively. Figure 31 shows the zenith angle distributions from Soudan-2 for events selected according to the above criteria (Mann, 1999). The shape of the zenith angle distribution for the CC ν_e sample agreed with the MC prediction. For the CC ν_μ sample, a deficit of upward-going events was clearly observed. However, a less significant deficit of down-going events was also observed. From Figure 31, $(U/D)_{Data}/(U/D)_{MC}$ for the CC ν_μ sample was $0.76 \pm 0.18(stat.)$. Although the statistics of the Soudan-2 data were limited, the observed zenith angle-dependent deficit of μ-like events was consistent with the Super-Kamiokande data.

We now summarize the systematic error in the $(U/D)_{Data}/(U/D)_{MC}$ measurement in Super-Kamiokande. A comparison of results from the Monte Carlo simulation using different flux models (Honda *et al.*, 1990, 1995; Agrawal *et al.*, 1996) as inputs resulted in an uncertainty of roughly $\pm 2 \sim 3\%$ in the expected U/D values for e-like and μ-like sub-GeV events, and less than $\pm 2\%$ for multi-GeV events. These two flux calculations did not assume the existence of the 1 km mountain over the Super-Kamiokande detector. The mountain reduces the neutrino flux because some fraction of muons are stopped before they decay in flight. The estimated effect of the presence of the mountain

was ±2% in U/D for the multi-GeV events. The effect was much smaller for the sub-GeV events. (The effect of the mountain over the detector should be larger for NUSEX, Frejus and experiments at Gran Sasso, and should be smaller for IMB, depending on the height of the mountain. See also Figure 11.) The estimated energy calibration difference between upward-going and downward-going particles was ±0.6% in Super-Kamiokande. This difference caused ±0.9%, and ±0.7% uncertainty in U/D for the multi-GeV e-like and μ-like events. This uncertainty is much smaller for the sub-GeV sample. A contamination from non-neutrino background such as downward-going cosmic ray muons could have directional correlation. The maximum contribution to the uncertainty in U/D from the background contamination was estimated to be ±1.2%, ±0.2%, ±0.4% and ±0.4% for the sub-GeV e-like, μ-like, multi-GeV e-like and μ-like events, respectively.

The $(U/D)_{Data}/(U/D)_{MC}$ values from various experiments are summarized in Figure 32. In the Super-Kamiokande (and the Kamiokande) data, $(U/D)_{Data}/(U/D)_{MC}$ for e-like events were consistent with the expectations. $(U/D)_{Data}/(U/D)_{MC}$ for high momentum μ-like events deviated significantly from unity, while $(U/D)_{Data}/(U/D)_{MC}$ for low momentum μ-like events was consistent with unity. In the momentum range below 400 MeV/c, the possible up-down asymmetry of the neutrino flux is largely washed out due to the poor angular correlation between the lepton and the neutrino directions (see Figure 28). Super-Kamiokande has found no detector bias differentiating e-like and μ-like events that could explain an asymmetry in μ-like events but not in e-like events (Fukuda *et al.*, 1998b). From these studies, Super-Kamiokande concluded that the observed up-down asymmetry cannot be due to a systematic effect in the data analysis, the detector, or the flux calculation.

6. East-west anisotropy

As we will show later, the zenith angle-dependent deficit of μ-like events is explained by neutrino oscillations. However before describing the neutrino oscillation analysis, we show another directional distribution, the azimuthal angle distribution.

The azimuthal anisotropy, called the east-west effect, was discovered in the 1930's as a deficit of secondary cosmic ray muons arriving from the easterly direction compared to a westerly direction (Johnson, 1933a, 1933b, 1935; see also, Rossi, 1964). Since the Earth has a magnetic field and the primary cosmic rays are positively charged, there is an angular anisotropy for those primaries which reach and interact in the atmosphere. The azimuthal anisotropy varies according to the position on the Earth and the momentum and charge of the primary cosmic ray. The anisotropy can be characterized by a cutoff rigidity, which is the minimum rigidity at which an incoming particle can reach the atmosphere. For example, at the Super-Kamiokande site, the cutoff momentum for downward-going protons is about 10 GeV/c, and for horizontally-arriving protons from the east it is about 50 GeV/c (see Figure 4). This effect should result in the depletion of the westward-going atmospheric neutrino flux. Since the mean path length of neutrinos should be independent of the azimuthal angle in a first approximation, the study of the azimuthal angle distribution should give useful information on the geomagnetic field effects independent of neutrino oscillations.

To study the azimuthal angle distribution, Super-Kamiokande selected events according to the following criteria: single-ring events with momentum between 400 MeV/c and 3000 MeV/c and with the cosine of zenith angle between −0.5 and 0.5. Figure 33 shows the azimuthal angle distributions for e-like and μ-like events observed in Super-Kamiokande during a 45 kton·yr exposure of the detector (Futagami *et al.*, 1999). An east-west anisotropy was observed and the observed anisotropy was consistent with the Monte Carlo prediction. In order to understand the magnitude of the east-west anisotropy quantitatively, the east-west asymmetry, $(N_E - N_W)/(N_E + N_W)$, was calculated. $N_E(N_W)$ represents the number of eastward-(westward-)going events. The observed asymmetries in e-like and μ-like events were 0.21±0.04 and 0.08±0.04, respectively. The corresponding Monte Carlo predictions were 0.13 and 0.11 for e-like and μ-like events, respectively.

The study of the azimuthal angle distributions, which should be unaffected by neutrino oscillations, showed that the data and the Monte Carlo were in good agreement for both e-like and μ-like events. This observation suggested that the geomagnetic field effects in the production of atmospheric neutrinos in the GeV energy range and the resolution for reconstructing the neutrino direction were reasonably well-modeled.

Finally we note that the observed asymmetry in e-like (μ-like) events was larger (smaller) than the prediction based on the one-dimensional flux calculation, although the discrepancies were not significant statistically. It has been pointed out that the possible discrepancies can be resolved by including the full three-dimensional features of the neutrino production in the flux calculation (Lipari, 2000b).

Because of the small (μ/e) ratio and the zenith angle-dependent deficit of μ-like events, Kamiokande, Super-Kamiokande and Soudan-2 carried out detailed neutrino oscillation analyses. In this section, the neutrino oscillation analysis from Super-Kamiokande is described. The results of the analyses from other experiments are also described.

Two-flavor $\nu_\mu \to \nu_e$ and $\nu_\mu \to \nu_\tau$ oscillation hypotheses were tested by a χ^2 comparison of the data and Monte Carlo, allowing all important Monte Carlo parameters to vary weighted by their expected uncertainties (Fukuda *et al.*, 1998c). The data were binned by particle type, momentum, and $\cos\Theta$. A χ^2 is defined as:

$$\chi^2 = \sum_{e \text{ or } \mu,\ cos\Theta,\ p}^{70} \left(\frac{N_{Data} - \alpha \cdot N_{MC}(\sin^2 2\theta, \Delta m^2, \epsilon_j)}{\sigma} \right)^2 + \sum_j^7 \left(\frac{\epsilon_j}{\sigma_j} \right)^2, \tag{3}$$

where the sum is over five bins equally spaced in $\cos\Theta$ and seven momentum bins for both e-like events and μ-like plus PC events (70 bins total). The statistical error, σ, accounts for both data statistics and the weighted Monte Carlo statistics. N_{Data} is the measured number of events in each bin. $N_{MC}(\sin^2 2\theta, \Delta m^2, \epsilon_j)$ is the expected number of Monte Carlo events and is a function of $\sin^2 2\theta$, Δm^2 and ϵ_j. α is an overall normalization factor. The uncertainty in the overall normalization was estimated to be 25%, however the absolute normalization was treated as a free parameter. The ϵ_j's are parameters which are related to the systematic uncertainties. σ_j is the uncertainty corresponding to each ϵ_j. The parameters (and their uncertainties) considered in this analysis were: E_ν spectral index (0.05), sub-GeV $(\mu/e)_{Data}/(\mu/e)_{MC}$ (8%), multi-GeV $(\mu/e)_{Data}/(\mu/e)_{MC}$ (12%), relative normalization of PC to FC (8%), L/E_ν (15%), sub-GeV (2.4%) and multi-GeV (2.7%) up-down ratios.

For $\nu_\mu \to \nu_e$, effects of matter on neutrino propagation through the Earth were included (Mikheyev and Smirnov, 1985, 1986; Wolfenstein, 1978). Due to the small number of events expected from τ-production (about 20 CC ν_τ events per 22.5 kton·year), the effects of τ appearance and decay were neglected in simulations of $\nu_\mu \to \nu_\tau$. A global scan was made on a $(\sin^2 2\theta, \log \Delta m^2)$ grid minimizing χ^2 with respect to the ϵ_j uncertainty parameters at each point.

For the test of $\nu_\mu \to \nu_\tau$ oscillations, the Super-Kamiokande data based on 61 kton·yr exposure gave a best-fit at $(\sin^2 2\theta, \Delta m^2) = (1.00,\ 2.6 \times 10^{-3}\ \text{eV}^2)$ inside the physical region $(0 \le \sin^2 2\theta \le 1)$. The χ^2 value at this point $(\chi^2_{min(phys)})$ was 45.4. The degrees of freedom (DOF) for this fit was 67, since there were 77 terms in Eq. (3), and the 7 uncertainty parameters (ϵ_j), the absolute normalization, $\sin^2 2\theta$ and Δm^2 were estimated by the fit. The best-fit values of the Monte Carlo uncertainty parameters were all within their expected errors for this point. If the unphysical region, $\sin^2 2\theta > 1.0$, was included in the analysis, the best-fit point was at $(1.01,\ 2.6 \times 10^{-3}\ \text{eV}^2)$. However, the difference in χ^2_{min} between unphysical and physical regions was only 0.1. The 90% C.L. allowed region was defined to be located within $\chi^2_{min(phys)} + 4.8$ based on the method described in Barnett *et al.*, (1996). The allowed region is shown in Figure 34. The χ^2 increases rapidly outside of the 90% C.L. region. $\chi^2 = 191/69$ DOF was obtained, when calculated at $\sin^2 2\theta = 0$, $\Delta m^2 = 0$ (i.e. assuming no oscillations).

For the test of $\nu_\mu \to \nu_e$ oscillations, the Super-Kamiokande data resulted in a relatively poor fit; $\chi^2_{min} = 89/67$ DOF, at $(\sin^2 2\theta, \Delta m^2) = (0.99,\ 3.5 \times 10^{-3}\ \text{eV}^2)$. The χ^2_{min} for $\nu_\mu \to \nu_e$ was larger than that for $\nu_\mu \to \nu_\tau$ by more than 40. For $\nu_\mu \to \nu_e$ oscillations, an excess of upward-going e-like events is expected. However, the Super-Kamiokande data did not show any significant excess for these directions (see Figure 29). Super-Kamiokande concluded that the $\nu_\mu \to \nu_e$ hypothesis was not favored. This conclusion was consistent with the non-observation of $\bar{\nu}_e \to \bar{\nu}_x$ oscillations ($x = \mu$ or τ) by the CHOOZ (Apollonio *et al.*, 1998, 1999) and Palo Verde (Boehm *et al.*, 2000) experiments.

In Figure 29, the zenith angle distributions for the sub- and multi-GeV samples observed by Super-Kamiokande are compared to the Monte Carlo expectation (no oscillations, solid lines) and the best-fit expectation for $\nu_\mu \to \nu_\tau$ oscillations (dashed lines). The oscillated Monte Carlo simulation well reproduces the zenith angle distributions of the data.

Figure 35 shows the expected $(\mu/e)_{Data}/(\mu/e)_{MC}$ values as a function of Δm^2. Figure 36 shows the expected U/D values as a function of Δm^2. The observed small $(\mu/e)_{Data}/(\mu/e)_{MC}$ and U/D values consistently suggest 10^{-3} to 10^{-2} eV^2 for Δm^2.

Because the neutrino oscillation probability is a function of L/E_ν, L/E_ν dependent deficit of μ-like events should be observed for $\nu_\mu \to \nu_\tau$ oscillations. Figure 37 shows the L/E_ν distributions for e-like and μ-like events. A clear deficit of μ-like events was observed for large L/E_ν ($\gtrsim$100 km/GeV), while the distribution for e-like events was consistent with flat. The observed deficit of μ-like events was well reproduced by the Monte Carlo simulation with neutrino oscillations.

The allowed regions obtained by the contained event analyses from Kamiokande (Fukuda *et al.*, 1994) and Soudan-2 (Mann, 1999) are also shown in Figure 34. The Super-Kamiokande allowed region favors a lower Δm^2 than does

Kamiokande. However, the allowed regions from both experiments have a region of overlap. One of the reasons for the difference in the allowed region is the zenith angle distribution of the sub-GeV μ-like events. The $(U/D)_{Data}/(U/D)_{MC}$ values of the μ-like events from Kamiokande and Super-Kamiokande are summarized in Figure 32. It should be noted that the Kamiokande $(U/D)_{Data}/(U/D)_{MC}$ value for the sub-GeV μ-like events was consistent with unity even in the momentum range of >500 MeV/c. However, Super-Kamiokande observed a smaller $(U/D)_{Data}/(U/D)_{MC}$ value for the same energy range. This difference resulted in a difference in the favored Δm^2 region for these two experiments, because the energy region for which $(U/D)_{Data}/(U/D)_{MC}$ is small is directly related to the determination of Δm^2.

B. Upward going muons

Energetic atmospheric ν_μ's passing through the Earth interact with rock surrounding the detector and produce muons via CC interactions. Upward going muons can be categorized into two types: "upward through-going muons" enter the detector and exit, and "upward stopping muons" enter the detector and stop inside it.

Muons produced by neutrino interactions can only be identified when traveling in the upward-going direction, where the background from cosmic ray muons is small. Careful studies of the background contamination have been carried out in atmospheric neutrino experiments. For example, the estimated contaminations from cosmic-ray muon background were 0.7% and 7% for the through-going muon and stopping muon samples, respectively, in Super-Kamiokande. The higher background contamination in the upward stopping muon sample compared to the through-going muon sample can be understood as being due to the larger multiple scattering effect in the lower energy region. These estimated background events were statistically subtracted from the analyses.

1. Upward through-going muons

The typical energy of a neutrino which produces an upward through-going muon is about 100 GeV (see Figure 18). Neutrinos arriving vertically travel roughly 13,000 km, while those coming from near the horizon travel only 500 km. These numbers, together with the Δm^2 region from the contained event analysis ($\sim 3 \times 10^{-3}$ eV^2), suggest that the neutrino oscillation effect can be seen in the zenith angle distribution of the upward through-going muon events. In other words, a larger deficit of vertically upward through-going muon events is expected than for almost horizontally-going muons.

In the past, several experiments observed these upward-going muons. The first atmospheric neutrino experiments observed these muons in the 1960's (Achar *et al.*, 1965a, 1965b; Reines *et al.*, 1965, 1971; Krishnaswamy *et al.*, 1971; Bergeson, Cassiday and Hendricks, 1973; Crouch *et al.*, 1978). Then in the late 1970's, a large scale experiment using liquid scintillators started at Baksan (Boliev *et al.*, 1981). In the 1980's, large detectors constructed for the detection of proton decay began to observe a large number of upward through-going muons.

The Baksan scintillator telescope has been in operation for about 20 years. They observed 424 upward through-going muons during 10.55 years of operation (Boliev *et al.*, 1995). The threshold energy of these muons was 1 GeV. The observed average flux was $2.72\times10^{-13}\ cm^{-2}sec^{-1}sr^{-1}$, while the expected flux was $2.62\sim2.94\times10^{-13}\ cm^{-2}sec^{-1}sr^{-1}$. A neutrino oscillation analysis was carried out by comparing the number of observed and expected events with $-1 < \cos\Theta < -0.6$ (vertically upward-going muons). No evidence for neutrino oscillations was observed.

The IMB experiment observed 532 upward through-going muon events during 3.6 years of detector operation (Becker-Szendy *et al.*, 1992a). No zenith angle distribution was reported. The threshold energy of these muons was 1.8(1.0) GeV for the initial 1/3 (later 2/3) of the data taking time. The expected number of events was $516\pm103(theo.)$, where *theo.* means the theoretical error in the prediction. Based on the comparison of the observed and expected number of events, IMB estimated an excluded region of neutrino oscillation parameters: Δm^2 higher than 2×10^{-3} eV^2 was excluded at 90% C.L. for $\sin^2 2\theta = 1$ and for $\nu_\mu \rightarrow \nu_\tau$ oscillations. However, we comment that the structure functions (Eichten *et al.* (EHLQ), 1984) used in their analysis predicted smaller cross sections than the data. Therefore, the excluded region is likely to have been over-estimated.

Kamiokande observed 372 upward through-going muons during 2456 detector live days. The selection criteria were: $-1 \leq \cos\Theta \leq -0.04$, where Θ is the zenith angle of the muon direction, and a track length of the muon in the inner detector of longer than 7 meters (Hatakeyama *et al.*, 1998). The minimum (mean) energy loss of these muons in the inner detector is 1.6(3.0) GeV. The average detection efficiency was 97%. With the requirement of $\cos\Theta < -0.04$, the background contamination was negligible. The observed average flux of upward-going muons was $1.94\pm0.10(stat.)^{+0.07}_{-0.06}(syst.)\times10^{-13}\ cm^{-2}sec^{-1}sr^{-1}$. The expected flux based on the calculated neutrino flux of

Agrawal *et al.* (1996) was $2.46\pm0.54(theo.) \times 10^{-13}\ cm^{-2}sec^{-1}sr^{-1}$. Figure 38 shows the zenith angle distribution of the upward through-going muon flux observed in Kamiokande.

In Super-Kamiokande, 1196 upward through-going muon events were observed during 1074 detector live days (Fukuda *et al.*, 1999a, 2000a). The selection criteria were: cosΘ <0, two outer detector clusters corresponding to the muon entrance and exit points, and the track length of the muon inside the inner detector of longer than 7 meters. The minimum (mean) energy loss of these muons in the inner detector is 1.6 (6) GeV. The average detection efficiency of these events was estimated to be >99%. The validity of this efficiency was tested using the real down-going cosmic-ray muons by assuming the up-down symmetry of the detector.

The number of background events, 8.6, was estimated by extrapolating the zenith angle distribution of cosmic ray muons with $0 \leq \cos\Theta \leq 0.08$. Background events were expected only in the $-0.1 \leq \cos\Theta \leq 0$ bin and were subtracted in further analyses. The observed average flux of upward going muons was $1.73\pm0.05(stat.)\pm0.02(syst.) \times 10^{-13}\ cm^{-2}sec^{-1}sr^{-1}$. The expected fluxes based on the calculated neutrino flux of Honda *et al.*, (1995) and Agrawal *et al.*, (1996) were $1.84\pm0.41(theo.)\times10^{-13}\ cm^{-2}sec^{-1}sr^{-1}$ and $1.97\pm0.44(theo.)\times10^{-13}\ cm^{-2}sec^{-1}sr^{-1}$, respectively. We note that the average energy loss of the upward through-going muons and therefore the average neutrino energy in Super-Kamiokande is higher than that in Kamiokande, resulting in a lower muon flux. Figure 39 shows the zenith angle distribution of the upward through-going muon flux observed in Super-Kamiokande.

The MACRO experiment observed 607 upward through-going muon events after a subtraction of 28 background events (Ambrosio *et al.*, 1998; Bernardini, 1999; Spurio, 1999). The predicted number of events was $825\pm140(theo.)$ based on the neutrino flux of Agrawal *et al.* (1996). (MACRO has not shown the average flux of the upward through-going muons.) Figure 40 shows the zenith angle distribution of the upward through-going muon flux observed in MACRO.

It has been argued by Lipari and Lusignoli (1998) that the prediction for the shape of the zenith angle distribution is accurate. The measured zenith-angle distributions in these three experiments had similar shapes: these experiments observed lower flux near the vertical direction compared with the predicted flux. The χ^2 values of the comparison of the shape of the zenith angle distributions of the data and prediction were 21.3/9 DOF, 22.9/9 DOF and 22.9/8 DOF for Kamiokande, Super-Kamiokande and MACRO, respectively.

Neutrino oscillation analyses were carried out by these experiments. In Kamiokande and Super-Kamiokande, the oscillation parameters were estimated using a χ^2 method:

$$\chi^2 = \sum_{cos\Theta}^{10} \left(\frac{\phi_{Data} - \alpha \cdot \phi_{MC}(\sin^2 2\theta, \Delta m^2)}{\sigma} \right)^2 + \left(\frac{\alpha - 1}{\sigma_\alpha} \right)^2, \tag{4}$$

where σ is the statistical and systematic error in the observed flux (ϕ_{Data}), and α and σ_α are the absolute normalization factor of the expected flux($\phi_{MC}(\sin^2 2\theta,\ \Delta m^2)$) and its uncertainty, respectively. σ_α was taken to be $\pm22\%$ by adding the theoretical uncertainty and correlated experimental errors. The uncertainty in the absolute neutrino flux ($\pm20\%$) was the dominant source of σ_α. A minimum χ^2 was calculated by changing α for each ($\sin^2 2\theta$, Δm^2). Since the contained event data preferred $\nu_\mu \rightarrow \nu_\tau$ oscillations and since the reactor neutrino oscillation experiments (Apollonio *et al.*, 1998, 1999; Boehm *et al.*, 2000) have excluded the $\nu_\mu \rightarrow \nu_e$ oscillation parameter region relevant to the atmospheric neutrino data, only $\nu_\mu \rightarrow \nu_\tau$ oscillations were tested.

The Kamiokande data had χ^2_{min} at $(\sin^2 2\theta, \Delta m^2) = (1.0, 3.2 \times 10^{-3}\ \mathrm{eV}^2)$ with α =1.00. The χ^2_{min} value was 12.8/8 DOF. χ^2_{min} for the Super-Kamiokande data occurred at $(\sin^2 2\theta, \Delta m^2) = (0.77, 1.3 \times 10^{-2}\ \mathrm{eV}^2)$ with α =1.13. The χ^2_{min} value was 10.3/8 DOF. The allowed regions did not change significantly for two assumed neutrino fluxes, (Honda *et al.*, 1995) and (Agrawal *et al.*, 1996), suggesting that the zenith angle and energy dependence of the calculated neutrino flux at high energies is well-understood.

The MACRO experiment carried out a similar analysis and found that the best fit point was in the region of $(\sin^2 2\theta, \Delta m^2) = (1.0, (a few) \times 10^{-3}\ \mathrm{eV}^2)$.

Figure 41 shows the allowed regions of neutrino oscillation parameters obtained from these upward going muon data. The allowed regions were larger than those of the contained events. However they overlapped the allowed regions obtained by the contained events. We note that the allowed region from MACRO was substantially smaller than those from Super-Kamiokande and Kamiokande. This can be understood (in part) by the fact that the χ^2_{min} value in the unphysical region (10.6) was smaller than the χ^2_{min} value in the physical region (12.5) (Bernardini, 1999), favoring large $\sin^2 2\theta$. Also, the estimated uncertainty of the absolute normalization of the upward through-going muon flux was smaller for the MACRO's analysis (17%) than for Super-Kamiokande and Kamiokande (22%). In addition, the statistical method adopted by the MACRO experiment (Feldman and Cousins, 1998), if applied to the upward-going muons with the oscillation parameter region suggested by the present atmospheric neutrino data, results in smaller

allowed region than that obtained based on the method adopted by Kamiokande and Super-Kamiokande (Barnett *et al.*, 1996).

Finally we comment that much larger detectors, AMANDA (Karle *et al.*, 1999) and BAIKAL (Balkanov *et al.*, 1999), have begun to observe upward-going muons. Since the threshold energies of the muons in these detectors are much higher than those in the detectors described in this section, the data from these detectors could be useful to study the atmospheric neutrinos in still higher energy regions.

2. Upward stopping muons

In large detectors such as Super-Kamiokande, a substantial fraction of upward going muons stop in the detector. The typical neutrino energy of the upward stopping muons is about 10 GeV, which is substantially lower than that of the upward through-going muons. Therefore, for some neutrino oscillation parameters, the observed (stopping/through-going) flux ratio of the upward-going muons should be different from the calculated ratio. The first systematic study of these stopping muons was carried out by the IMB experiment (Becker-Szendy *et al.*, 1992a). IMB found that the number of the observed events was in agreement with the Monte Carlo prediction, and obtained an excluded region of the neutrino oscillation parameters. However, it was found that a careful evaluation of the neutrino interaction cross section in the multi-GeV energy range increases the number of predicted upward stopping muon events (Lipari, Lusignoli, and Sartogo, 1995). It is likely that the excluded region was overestimated, and therefore we do not refer to this excluded region in this article.

Super-Kamiokande observed 285 upward stopping muons during 1053 detector live days (Fukuda *et al.*, 1999b, 2000a). The selection criteria were similar to those for upward through-going muons, except for a requirement of one outer detector cluster corresponding to the entrance point. The detection efficiency was estimated to be 99%. The estimated number of cosmic-ray background events was 20. It was estimated that these background events were mostly in the $-0.2 < \cos\Theta < 0$ bin. The background events were subtracted from this bin for further analyses. The resulting (stopping/through-going) flux ratio ($\equiv \Re$) of the data was $\Re = 0.226 \pm 0.016(stat.)^{+0.012}_{-0.010}(syst.)$, while the predicted value was $\Re = 0.37^{+0.049}_{-0.044}(theo.)$. The observed value was 2.9 σ smaller than the prediction. Figure 42 shows the zenith angle dependence of the observed $\Re$ together with the predictions with and without neutrino oscillations. Figure 39 shows the zenith angle distribution of the upward stopping muon flux. Also shown in the same figure are the predicted fluxes with and without neutrino oscillations. Clearly, the predicted flux and $\Re$ without neutrino oscillations disagree with the data beyond the systematic uncertainty of the predictions.

The 90% C.L. allowed region of the neutrino oscillations was estimated by a χ^2 test:

$$\chi^2 = \sum_{cos\Theta}^{5} \left(\frac{\Re_{Data} - \beta \cdot \Re_{MC}(\sin^2 2\theta, \Delta m^2)}{\sigma} \right)^2 + \left(\frac{\beta - 1}{\sigma_\beta} \right)^2, \tag{5}$$

where σ is the experimental (mostly statistical) error in the observed ratio ($\Re_{Data}$) and β and σ_β are the uncertainty factor of the expected ratio ($\Re_{MC}(\sin^2 2\theta, \Delta m^2)$) and its 1σ error, respectively. σ_β was taken to be $\pm 14\%$ by adding the theoretical uncertainty and correlated experimental systematic errors. The largest source of σ_β, 13%, was the uncertainty in the energy spectrum index of the atmospheric neutrino flux ($E_\nu^{\pm 0.05}$).

χ^2_{min} occurred at $(\sin^2 2\theta, \Delta m^2) = (1.0, 3.8 \times 10^{-3}\ \mathrm{eV}^2)$. Figure 41 shows the allowed region obtained from this analysis. Again, the allowed region was larger than that from the contained events. However it overlapped the allowed regions obtained by the contained and upward through-going muon data.

Before finishing this section, we mention the MACRO data on (upward stopping muons + downward PC events) and upward PC events (Spurio, 1999). MACRO has some ambiguity in separating upward stopping muon events and downward PC events, and therefore these events are combined. Assuming a 50%(0%) deficit of upward-(downward-)going events by neutrino oscillations, about 25% and 50% deficits are expected in the (upward stopping muons + downward PC) and upward PC samples, respectively. Figure 43 shows the zenith angle distributions of these events. The smaller numbers of events near the horizon are due to the detector geometry and the detection efficiency. Deficits of these events were observed in these samples, and were consistent with neutrino oscillations.

C. Combined analysis of contained events and upward-going muon events

We have seen that the contained and the upward-going muon events were consistent with neutrino oscillations. It is then a natural extension of the previous analyses to obtain an allowed region of neutrino oscillation parameters

by combining the contained and upward-going muon events. Kamiokande and Super-Kamiokande carried out these analyses.

The analysis method was similar to that for the contained events (see Eq. 3) and for the upward through-going muon events (see Eq. 4). The relative normalization between the contained events and upward-going muon events was considered as an additional constraint to the fit. The allowed regions obtained from these analyses are shown in Figure 44. As expected, with more constraints, the allowed regions are smaller than those obtained from the individual data sets. The χ^2 value of the neutrino oscillation analysis for the Super-Kamiokande data (61 kton·yr, 1053 day, and 1074 day data for the contained events, upward stopping muons, and upward through-going muons, respectively) at the best-fit parameter point ($\sin^2 2\theta = 1.00$ and $\Delta m^2 = 2.8\times10^{-3}$ eV^2) was 61.1 for 82 DOF. Even if the analysis was extended to the unphysical region ($\sin^2 2\theta > 1.0$), the best-fit parameter remained unchanged. The χ^2 value for no oscillation was 233 for 84 DOF, thus excluding the no oscillation hypothesis at a very high confidence level. Since the best-fit parameter set was in the physical region, the 90% C.L. allowed region was defined to be located within $\chi^2_{min}+4.6$. The 90% C.L. allowed parameter region from Super-Kamiokande was: $\sin^2 2\theta \geq 0.88$ and $2\times10^{-3} \leq \Delta m^2 \leq 5\times10^{-3}$ eV^2. We would like to point out that it is really remarkable that atmospheric neutrino events which range between $\sim$0.1 and $\sim10^3$ GeV in energy and $\sim$10 and $\sim10^4$ km in flight length are consistently explained by neutrino oscillations.

Finally, we comment that it is possible that the above allowed parameter region, especially in Δm^2, could shift slightly if a three-dimensional flux calculation is used for the prediction. Such a shift is possible because the three-dimensional flux calculation predicts an enhancement of the horizontal flux in the sub-GeV energy region (Battistoni *et al.*, 2000; Lipari, 2000a) relative to the flux based on the one-dimensional calculations. However this horizontal enhancement is not expected to change the predicted zenith-angle distribution for e-like and μ-like events significantly due to the large scattering angle in the low energy region (see Figure 28). Also, in the three-dimensional flux calculation, the distribution of the flight lengths of the neutrinos for the horizontal direction is predicted to be shorter by about 30% in the sub-GeV energy region (Battistoni *et al.*, 2000) relative to that based on the one-dimensional calculations.

D. Three-flavor neutrino oscillation analysis

Since there are three neutrino flavors, there should be three neutrino mixing angles, θ_{12}, θ_{13} and θ_{23} and one CP phase. The flavor neutrino states can be expressed as a superposition of the mass eigenstates as follows:

$$|\nu_\alpha\rangle = \sum_i U_{\alpha i}\,|\nu_i\rangle, \tag{6}$$

where U is a unitary mixing matrix which relates flavor eigenstates and mass eigenstates of neutrinos. α and i represent the flavor and mass eigenstates, respectively. The mixing matrix for three neutrinos (neglecting the CP term) can be expressed as:

$$U = \begin{pmatrix} c_{12}c_{13} & s_{12}c_{13} & s_{13} \\ -s_{12}c_{23} - c_{12}s_{23}s_{13} & c_{12}c_{23} - s_{12}s_{23}s_{13} & s_{23}c_{13} \\ s_{12}s_{23} - c_{12}c_{23}s_{13} & -c_{12}s_{23} - s_{12}c_{23}s_{13} & c_{23}c_{13} \end{pmatrix}, \tag{7}$$

where s_{ij} and c_{ij} $(i,j=1,2,3)$ show $\sin\theta_{ij}$ and $\cos\theta_{ij}$, respectively, and θ_{ij} is the mixing angle between the i-th and j-th generation neutrinos.

Also, there should be three Δm^2's. (Among them only two Δm^2's are independent.) However, a complete exploration of the three-flavor neutrino parameter space would be extremely complicated. Therefore, in the analysis of the atmospheric neutrino data, an approximation is commonly used to simplify the analysis (Fogli, Lisi and Montanino, 1997). The solar neutrino deficit is commonly interpreted as $\nu_e \to \nu_\mu$ oscillations with $|m_2^2 - m_1^2| \equiv \Delta m_{12}^2 \ll 10^{-4}$ eV^2, where m_i represents the mass of ν_i. If we assume $\Delta m_{12}^2 \ll 10^{-4}$ eV^2 and $\Delta m_{23}^2 (\equiv |m_3^2 - m_2^2|) \gtrsim 10^{-3}$ eV^2, atmospheric neutrino oscillations depend only on $\Delta m^2 (\equiv \Delta m_{23}^2 \simeq \Delta m_{13}^2)$. (However, for larger Δm_{12}^2 values, there should be a non-negligible effect of Δm_{12}^2 on atmospheric neutrino oscillations. See for example, Fogli, Lisi and Montanino, 1995; Peres and Smirnov, 1999).

With the above approximation, the neutrino oscillation probabilities in vacuum take the simple form:

$$P(\nu_\beta \to \nu_\alpha) = 4|U_{\alpha 3}|^2|U_{\beta 3}|^2 \sin^2\left(\frac{1.27\Delta m^2 L}{E_\nu}\right) \qquad (\alpha \neq \beta), \tag{8}$$

$$P(\nu_\alpha \to \nu_\alpha) = 1 - 4|U_{\alpha 3}|^2(1 - |U_{\alpha 3}|^2)\sin^2\left(\frac{1.27\Delta m^2 L}{E_\nu}\right). \quad (9)$$

For example, for $\nu_\mu \to \nu_\mu$, the oscillation probability is:

$$P(\nu_\mu \to \nu_\mu) = 1 - 4|s_{23}c_{13}|^2(1 - |s_{23}c_{13}|^2)\sin^2\left(\frac{1.27\Delta m^2 L}{E_\nu}\right). \quad (10)$$

If θ_{13} =0, the oscillation can be identified as pure two-flavor $\nu_\mu \to \nu_\tau$ oscillations with $\sin^2 2\theta \equiv 4s_{23}^2 c_{23}^2$.

In the absence of CP violating effects, the oscillation probabilities in vacuum are equal for neutrinos and anti-neutrinos. However, in matter these probabilities are not equal, and the probability must be calculated numerically for the Earth density profile (Wolfenstein, 1978; Mikheyev and Smirnov, 1985, 1986). We note that there has been a lot of theoretical work on the matter effect in the Earth (see for example, Pantaleone, 1998; Barenboim and Scheck, 1999; Chizhov and Petcov, 1999; Akhmedov, 1999; Akhmedov *et al.*, 1999).

Three-flavor analyses of the atmospheric neutrino data has been carried out by various authors (for a recent reference, see for example, Yasuda, 1998; Fogli *et al.*, 1999a; Sakai and Teshima, 1999; Meier and Ohlsson, 1999). The results can be summarized as follows. Since the shape of the observed zenith-angle distributions for e-like events is consistent with the Monte Carlo prediction, there is no evidence for non-zero θ_{13}. This result is consistent with the results from CHOOZ and Palo Verde which did not observe any oscillation effect (Apollonio *et al.*, 1998, 1999; Boehm *et al.*, 2000). The constraint on θ_{13} from the CHOOZ data is much stronger than that from the atmospheric neutrino data. Therefore, it is concluded that atmospheric neutrino oscillations are consistent with pure $\nu_\mu \to \nu_\tau$ and the result from the two-flavor oscillation analysis is approximately correct. For further details of the three-flavor analysis, see the original references.

VI. OTHER INTERPRETATIONS

An important question to ask is whether neutrino oscillations (generated by neutrino mass and mixing) are the only possible explanation of the atmospheric neutrino data. In this section, we review some of the alternative explanations of the atmospheric neutrino data. Most of the alternatives have already been excluded for various reasons.

A. Proton decay $p \to e^+\nu\nu$

Proton decay, $p \to e^+\nu\nu$, was proposed (Mann, Kafka and Leeson, 1992) to explain the small (μ/e) ratio. If protons decay into $e^+\nu\nu$ with the lifetime of about 4×10^{31}years, experiments should observe an excess of e-like events below about 500 MeV, thus explaining the small (μ/e) ratio. However, this scenario was essentially ruled out by the small (μ/e) ratio in the multi-GeV energy range and especially by the zenith angle-dependent deficit of μ-like events observed in Kamiokande(Fukuda *et al.*, 1994) and Super-Kamiokande (Fukuda *et al.*, 1998b, 1998c). Also, the high-statistics Super-Kamiokande data do not show any significant excess of e-like events below 500 MeV/c relative to the predicted momentum distribution (see Figure 26).

B. Neutron background

If there is a high flux of energetic neutrons at a detector site, a fraction of these neutrons enter into the fiducial volume of the detector and interact with the detector material producing energetic hadrons (mostly pions). A π^0 produced by this mechanism should look like an e-like event, if one of the two gammas is not detected. Such neutron background was suggested to explain the small (μ/e) ratio (Ryazhskaya, 1994, 1995).

The vertex position of these background events should cluster near the surface of the fiducial volume, because of the relatively short interaction length of neutrons. By using the vertex position distribution, it is possible to separate the neutrino and neutron events statistically. Figure 45 (left) shows the invariant mass distribution for events with 2 e-like Cherenkov rings observed in Kamiokande. A clear π^0 mass peak was observed. Figure 45 (right) shows the distribution of the distance from the nearest PMT plane for π^0-like events observed in Kamiokande. No evidence for background contamination was observed. From this figure Kamiokande concluded that the neutron background contamination should be less than 1.2% at 90% C.L. for the sub-GeV e-like sample (Fukuda *et al.*, 1996b). A similar analysis for the multi-GeV sample was carried out, finding no evidence for background contamination (Fukuda *et al.*,

1996b). Even stronger limits on the background were obtained by Super-Kamiokande. Because of the thicker anti-counter and because of the higher statistics, the upper limits on the neutron contamination in the sub- and multi-GeV e-like samples were estimated to be 0.1 and 0.2%, respectively (Fukuda *et al.*, 1998a, 1998b). These measurements ruled out neutron background contamination as an explanation for the small (μ/e) ratio.

C. $\nu_\mu \rightarrow \nu_{sterile}$ neutrino oscillations

The atmospheric neutrino data were consistent with $\nu_\mu \rightarrow \nu_\tau$ oscillations. However, since the expected event rate of ν_τ interactions in the contained event sample is small (about 20 fully contained CC ν_τ events are expected per 22.5kton·year, which is less than 1% of the total atmospheric neutrino events), and since most of the neutral-current (NC) events are eliminated from the analysis of neutrino oscillations using contained events, the contained event data could also be explained by $\nu_\mu \rightarrow \nu_{sterile}$ neutrino oscillations. $\nu_{sterile}$ is a hypothetical neutrino-like particle which does not interact with matter by either CC or NC weak interactions. Indeed, according to the neutrino oscillation analysis using contained events, both $\nu_\mu \rightarrow \nu_\tau$ and $\nu_\mu \rightarrow \nu_{sterile}$ were equally allowed (Foot, Volkas and Yasuda, 1998). Since the existence of $\nu_{sterile}$ has significant impacts on particle physics and cosmology, it must be studied seriously whether $\nu_\mu \rightarrow \nu_{sterile}$ oscillations are really favored by the atmospheric neutrino data.

There have been several suggestions for discriminating the two possibilities. One possibility is the (NC/CC ν_e) ratio, where NC and CC ν_e are the number of NC and CC ν_e events, respectively. If the oscillations are $\nu_\mu \rightarrow \nu_\tau$, the above ratio for the data should agree with the non-oscillated Monte Carlo prediction. On the other hand, if the oscillations are $\nu_\mu \rightarrow \nu_{sterile}$, the above ratio for the data should be smaller than the prediction for the non-oscillated Monte Carlo. π^0-like events were observed in Kamiokande (Fukuda *et al.*, 1996b) and Super-Kamiokande. For example, the π^0 data from Kamiokande are shown in Figure 45. A significant fraction of them (>85%) are NC events. As the (NC/CC ν_e) ratio, Super-Kamiokande took the π^0/sub-GeV-e-like ratio. The preliminary result on this ratio based on the 61 kton·yr data was (Fukuda *et al.*, 2000b): $(\pi^0/\text{sub-GeV-}e\text{-like})_{Data}$ / $(\pi^0/\text{sub-GeV-}e\text{-like})_{MC}$ = 1.02 $\pm 0.06(stat.)$ $\pm 0.23(syst.)$. The largest source of systematic error was the uncertainty in the NC π^0 production cross section. Because of the large systematic error, both hypotheses were allowed.

Other possibilities include studies of the zenith angle distributions of NC π^0 events (Learned, Pakvasa and Stone, 1998) or of multi-ring events which include a significant number of NC events (Hall and Murayama, 1998).

Another suggestion was that the matter effect for upward-going neutrino events could be useful to discriminate the two possibilities (see for example, Liu, Mikheyev and Smirnov, 1998; Lipari and Lusignoli, 1998a; see also, Akhmedov, Lipari and Lusignoli, 1993). In the case of $\nu_\mu \rightarrow \nu_\tau$ oscillations, the matter effect does not change the oscillation probability. On the other hand, in the case of $\nu_\mu \rightarrow \nu_{sterile}$ oscillations, the matter effect may change the oscillation probability significantly. For $\Delta m^2 \sim 3 \times 10^{-3}\text{eV}^2$, the neutrino oscillation probability is expected to be significantly modified only for high energy atmospheric neutrinos traveling through the Earth.

A preliminary result from Super-Kamiokande (Fukuda *et al.*, 2000c) was obtained from analyses of multi-ring, high-energy PC and upward through-going muon events. Multi-ring events with (a) the most energetic ring being e-like and (b) E_{vis} >400 MeV were used. The estimated fraction of NC events (in the absence of neutrino oscillations) was 29%. Figure 46(a) shows the zenith angle distribution of these events, together with the neutrino oscillation predictions. The difference between the two hypotheses for the expected zenith-angle distributions is significant at $\cos\Theta < -0.4$. In order to minimize the systematic error, the up-down ratio, $Up(-1 < cos\Theta < -0.4)/Down(0.4 < cos\Theta < 1)$, was studied. Figure 46(c) shows the expected up-down ratio as a function of Δm^2 for the two hypotheses, together with the ratio for the data. The ratio for the $\nu_\mu \rightarrow \nu_{sterile}$ neutrino oscillation hypothesis did not agree with the data by >2 standard deviations in the suggested Δm^2 range.

The typical neutrino energy for upward through-going muon events is about 100 GeV. Figure 46(b) shows the zenith angle distribution of these events, together with neutrino oscillation predictions. The difference between the two hypotheses for the zenith angle distributions is significant at $\cos\Theta < -0.4$. Therefore, the vertical-horizontal ratio, $Vertical(-1 < cos\Theta < -0.4)/Horizontal(-0.4 < cos\Theta < 0)$, of the flux was studied. Figure 46(d) shows the expected vertical-horizontal ratio as a function of Δm^2 for the two hypotheses, together with the ratio of the data. Since the expected vertical-horizontal ratio may depend on the flux calculation, the systematic error in the predicted ratio was carefully evaluated. A preliminary result by Honda, Kasahara and Midorikawa (1999) showed that the systematic error in this ratio from the flux calculation is less than 3% (see also, Lipari and Lusignoli, 1998). The total systematic error in the ratio was 3.3%. The expected vertical-horizontal ratio for the $\nu_\mu \rightarrow \nu_{sterile}$ neutrino oscillation hypothesis did not agree with the data by >2 standard deviations for a wide range of Δm^2. In addition, a similar analysis of high-energy PC events did not favor $\nu_\mu \rightarrow \nu_{sterile}$ neutrino oscillation hypothesis.

Finally, the two oscillation hypotheses were tested by combining these three studies by a χ^2 method:

$$\chi^2 = \chi^2_{multi-ring} + \chi^2_{PC} + \chi^2_{upgoing-muon}.$$

If the above χ^2 value is larger than 6.3 (11.3), the hypothesis is disfavored at 90 (99)% C.L.. Figure 47 shows the results of this hypothesis test. Because the matter effect and therefore the neutrino oscillation probability depend on $(m_j^2 - m_i^2)$ rather than $|m_j^2 - m_i^2|$ for $\nu_\mu \to \nu_{sterile}$ oscillations, both positive and negative $\Delta m^2 (\equiv m_j^2 - m_i^2)$ were tested. The $\nu_\mu \to \nu_\tau$ oscillation hypothesis did not contradict the data in this analysis. On the other hand, most of the parameter regions suggested by the analysis of FC events for the $\nu_\mu \to \nu_{sterile}$ hypothesis were disfavored at 99% C.L.(preliminary).

D. Neutrino decay

If ν_μ's decay to some other particles, the atmospheric neutrino data, the small $(\mu/e)_{Data}/(\mu/e)_{MC}$ ratio and the deficit of upward going ν_μ events, could be explained. However, a simple decay model, i.e., $P(\nu_\mu \to \nu_\mu) = e^{-\alpha L/E_\nu}$, where $\alpha = m_\nu/\tau_\nu$ and τ_ν is the neutrino lifetime, cannot explain the weak energy dependence of the small $(\mu/e)_{Data}/(\mu/e)_{MC}$ ratio observed in Kamiokande and Super-Kamiokande (see, Figures 26, 27). Therefore, a simple decay model is ruled out.

A neutrino decay-mixing explanation for the atmospheric neutrino data has been proposed (Barger *et al.*, 1999a, 1999b). Assuming $\nu_\mu = \cos\theta\nu_2 + \sin\theta\nu_3$ with $m_2 > m_3$, and ν_2 unstable and decaying to (anti-)ν_3 plus another particle, the ν_μ survival probability can be written as:

$$P(\nu_\mu \to \nu_\mu) = \sin^4\theta + \cos^4\theta e^{-\alpha L/E_\nu} + 2\sin^2\theta\cos^2\theta e^{-\alpha L/2E_\nu}\cos(\frac{\Delta m^2_{23} L}{2E_\nu}), \quad (11)$$

where $\alpha = m_2/\tau_{\nu 2}$. In this scenario, Δm^2_{23} must be larger than 0.73 eV^2 to satisfy constraints from kaon decay (Barger *et al.*, 1999a). Then the third term in the above equation averages to zero for atmospheric neutrinos. It was shown that the L/E_ν distribution of the Super-Kamiokande data can be explained reasonably well if $\cos^2\theta \sim 0.87$ and $\alpha \sim 1$ GeV$/D_E$, where $D_E = 12800$ km is the diameter of the Earth (Barger *et al.*, 1999a). However, soon after this proposal, it was shown that the fit to the higher energy events (especially the upward going muons) was poor (Lipari and Lusignoli, 1999; Fogli, Lisi and Marrone, 1999; Choubey and Goswami, 1999).

Another decay-mixing model has been proposed (Barger *et al.*, 1999a, 1999b), in which ν_μ is a mixed state of ν_2 and ν_3, and ν_2's decay into another state with which ν_2's do not mix. For example, this state could be a sterile neutrino. In this scenario, Δm^2_{23} does not need to satisfy >0.73 eV^2 and could be very small (Barger *et al.*, 1999a). In this case, $\cos(\frac{\Delta m^2_{23} L}{2E_\nu})$ in the third term of the above equation is approximately unity, and therefore $P(\nu_\mu \to \nu_\mu) = (\sin^2\theta + \cos^2\theta e^{-\alpha L/2E_\nu})^2$. It was shown that the atmospheric neutrino data including the upward-going muons can be explained (Barger *et al.*, 1999b). This model is difficult to distinguish from oscillations unless the dependence on L/E_ν is found to be exponential (decay-mixing model) or sinusoidal (oscillation). Finally, we comment that, in general, it will be important for future experiments to observe the sinusoidal L/E_ν dependence of $P(\nu_\mu \to \nu_\mu)$ to exclude many of the non-oscillation scenarios.

E. Non-standard neutrino oscillations

Possible non-standard neutrino interactions or properties can also generate neutrino oscillations. There have been several proposals for such mechanisms. A list of possibilities can be found in (Lipari and Lusignoli, 1999; Fogli *et al.*, 1999b). We will not go into the details of these models, although we mention that in many such models, the energy dependence of the oscillation probability does not take the form, $P(\nu_\mu \to \nu_\mu) = \alpha\cdot\sin(\beta \cdot L \cdot E_\nu^{-1})$, where α and β are constants. Instead, some of the models take the form, $P(\nu_\mu \to \nu_\mu) = \alpha\cdot\sin(\beta \cdot L \cdot E_\nu^n)$, where $n = 0$ or 1.

Since the atmospheric neutrino data cover the energy range from about 0.1 GeV to 10^3 GeV, the energy dependence of the oscillation can be studied in detail. The Super-Kamiokande data based on 500 days of the detector exposure were analyzed in (Fogli *et al.*, 1999b). In this analysis, FC, PC and upward-going muon events were used. The data were fitted with n as a free parameter. It was found that $n = -0.9 \pm 0.4$ at 90% C.L., thus essentially excluding

non-standard oscillation models which take either $n = 0$ or 1. A similar conclusion was obtained in (Lipari and Lusignoli, 1999).

Some of the non-standard neutrino oscillations cannot be described by $P(\nu_\mu \to \nu_\mu) = \alpha \cdot \sin(\beta \cdot L \cdot E_\nu^n)$. An important example of such a model is neutrino oscillations generated by flavor changing neutral currents (FCNC) (Gonzalez-Garcia *et al.*, 1999). In this case, the L/E_ν in the mass-generated neutrino oscillation is replaced by the column density. In this model, there is no energy dependence in the oscillations. Furthermore, since air has a density much lower than that of the Earth, down-going neutrinos are essentially unaffected. Therefore, the neutrino oscillation probability is a function of zenith angle only. A detailed analysis of the atmospheric neutrino data in terms of FCNC was carried out in (Lipari and Lusignoli, 1999; Fornengo, Gonzalez-Garcia, and Valle, 1999). They observed that this model was essentially ruled out because, among other reasons, the observed upward through-going muons had a deficit considerably smaller than the deficit of upward-going stopping muons and upward-going multi-GeV muons.

VII. SUMMARY AND FUTURE PROSPECT

In the past several decades, atmospheric neutrinos have been observed by various experiments. Until 1988, the study of atmospheric neutrinos was a relatively quiet field. After 1988, when Kamiokande reported an experimental study of the flavor ratio of the atmospheric neutrino fluxes, various experimental and flux calculation studies were carried out to understand the details of the atmospheric neutrinos. The understanding of the atmospheric neutrino phenomena improved significantly after Super-Kamiokande started taking data in 1996.

The total number of atmospheric neutrino events observed by various atmospheric neutrino detectors is about 1×10^4 as of this writing. Remarkably, these data, which vary from 10 km to 10^4 km in flight length and from 0.1 GeV to 10^3 GeV in energy, are consistently explained by two-flavor $\nu_\mu \to \nu_\tau$ neutrino oscillations. The most convincing evidence for neutrino oscillations came from the zenith angle distribution of the multi-GeV μ-like data from Super-Kamiokande. The data showed nearly a factor of two deficit of upward-going events relative to the downward-going ones, where up-down symmetry was expected. The 90% C.L. allowed region of the neutrino oscillation parameters obtained from Super-Kamiokande was: 2×10^{-3} eV$^2 < \Delta m^2 < 5 \times 10^{-3}$ eV^2 and $\sin^2 2\theta > 0.88$. We conclude that the present data from various atmospheric neutrino experiments give evidence for neutrino oscillations.

The study of neutrino oscillations by the atmospheric neutrinos is maturing from the discovery phase to the precision measurement phase. To determine the neutrino oscillation parameters more accurately, improvements in both the data quality and the flux calculation are required. There is now intense flux calculation activity in which the fluxes are calculated based on the full three-dimensional simulation of the particle trajectory and the Earth. As the full three-dimensional calculation predicts an enhancement of horizontal fluxes in the sub-GeV energy region, the estimated Δm^2 based on the comparison of the data and the one-dimensional flux calculation may be shifted (slightly). In spite of the possible correction to the Δm^2 value, the measurement of $\sin^2 2\theta$ by atmospheric neutrinos is likely to be robust, and independent of the details of the flux calculation. The accuracy of the $\sin^2 2\theta$ measurement has not yet been limited by the systematic uncertainties.

Several neutrino oscillation experiments using high-energy accelerators and very long neutrino flight distances (250 km (the K2K experiment, Nishikawa, 1998) or 730 km (the MINOS project, Wojcicki, 1998; a long baseline project between CERN and Grand Sasso, Picchi and Pietropaolo, 1998)) will provide various important data. These experiments will study muon-neutrino oscillations intensively. These experiments will be able to determine the Δm^2 value much more precisely than for atmospheric neutrinos due to the well-defined neutrino flight distance. While the atmospheric neutrino data favor $\nu_\mu \to \nu_\tau$ rather than $\nu_\mu \to \nu_{sterile}$, the signal of ν_τ CC interaction has not been observed. Some of the long baseline experiments will be able to observe direct evidence for $\nu_\mu \to \nu_\tau$ oscillations via the observation of ν_τ CC events.

Finally, we note that solar neutrino experiments are also very important to explore neutrino oscillations involving ν_e. The study of neutrino oscillations will continue to be an important and exciting field.

ACKNOWLEDGEMENTS

We gratefully acknowledge the Super-Kamiokande and Kamiokande members for their useful discussions, suggestions and help. A substantial fraction of the data described in this article are from these experiments. We would like to thank especially E. Kearns for useful discussions, and J. Kameda, K. Kaneyuki, M. Messier, M. Shiozawa, C. Saji, M. Takita and T. Toshito for producing some figures used in this article. We also would like to thank K. Scholberg

for the careful reading of this article. We acknowledge P. Lipari for useful discussions and comments. This work is supported by the Japanese Ministry of Education, Science, Sports and Culture.

REFERENCES

Abdurashitov, J. N., *et al.*, 1999, Phys. Rev. Lett. **83**, 4686.
Achar, C. V., *et al.*, 1965a, Phys. Lett. **18**, 196.
Achar, C. V., *et al.*, 1965b, Phys. Lett. **19**, 78.
Aglietta, M., *et al.*, 1989, Europhys. Lett. **8**, 611.
Agrawal, V., *et al.*, 1996, Phys. Rev. D **53**, 1314.
Ahlen, S., *et al.*, 1993, Nucl. Inst. Meth. A **324**, 337.
Akhmedov, E., P. Lipari, and M. Lusignoli, 1993, Phys. Lett. B **300**, 128.
Akhmedov, E. Kh., 1999, Nucl. Phys. B **538**, 25.
Akhmedov, E. Kh., *et al.*, 1999, Nucl. Phys. B **542**, 3.
Allison, W. W. M., *et al.*, 1996a, Nucl. Inst. Meth. A **376**, 36.
Allison, W. W. M., *et al.*, 1996b, Nucl. Inst. Meth. A **381**, 385.
Allison, W. W. M., *et al.*, 1998, Phys. Lett. B **427**, 217.
Allison, W. W. M., *et al.*, 1999, Phys. Lett. B **449**, 137.
Allkofer, O. C., K. Carstensen, and W. D. Dau, 1971, Phys. Lett. **36B**, 425.
Ambrosio, M., *et al.*, 1998, Phys. Lett. B **434**, 451.
Anikeev, V. B., *et al.*, 1996, Z. Phys. C **70**, 39.
Apollonio, M., *et al.*, 1998, Phys. Lett. B **420**, 397.
Apollonio, M., *et al.*, 1999, Phys. Lett. B **466**, 415.
Arisaka, K., *et al.*, 1985, J. Phys. Soc. Jpn. **54**, 3213.
Astier, P., *et al.*, 1999, Phys. Lett. B **453**, 169.
Athanassopoulos, C., *et al.*, 1995, Phys. Rev. Lett. **75**, 2650.
Athanassopoulos, C., *et al.*, 1996a, Phys. Rev. C **54**, 2685.
Athanassopoulos, C., *et al.*, 1996b, Phys. Rev. Lett. **77**, 3082.
Athanassopoulos, C., *et al.*, 1998, Phys. Rev. Lett. **81**, 1774.
Bahcall, J. N., S. Basu, and M. H. Pinsonneault, 1998, Phys. Lett. B **433**, 1.
Bahcall, J. N., P. I. Krastev, and A. Yu. Smirnov, 1998, Phys. Rev. D **58**, 096016.
Balkanov, V. A., *et al.*, 1999, Astropart. Phys. **12**, 75.
Barger, V., *et al.*, 1980, Phys. Lett. **93B**, 194.
Barger, V., K. Whisnant, and R. J. N. Phillips, 1980, Phys. Rev. D **22**, 1636.
Barger, V., and K. Whisnant, 1988, Phys. Lett. B **209**, 365.
Barger, V., *et al.*, 1999a, Phys. Rev. Lett. **82**, 2640.
Barger, V., *et al.*, 1999b, Phys. Lett. B **462**, 109.
Barenboim, G. and F. Scheck, 1999, Phys. Lett. B **450**, 189.
Barnett, R. M., *et al.*, 1996, Phys. Rev. D **54**, 375; Based on a two-dimensional extension of the method in Review of Particle Properties, Section: Error and confidence intervals – Bounded physical region.
Barr, G., and T. K. Gaisser, and T. Stanev, 1989, Phys. Rev. D **39**, 3532.
Barr, S., *et al.*, 1988, Phys. Lett. B **214**, 147.
Bartelt, J., *et al.*, 1983, Phys. Rev. Lett. **50**, 651.
Battistoni, G., *et al.*, 1982, Phys. Lett. **118B**, 461.
Battistoni, G., *et al.*, 1983, Phys. Lett. **133B**, 454.
Battistoni, G., *et al.*, 1986, Nucl. Inst. Meth. A **245**, 277.
Battistoni, G., *et al.*, 2000, Astropart. Phys. **12**, 315.
Becker-Szendy, R., *et al.*, 1990, Phys. Rev. D **42**, 2974.
Becker-Szendy, R., *et al.*, 1992, Phys. Rev. D **46**, 3720.
Becker-Szendy, R., *et al.*, 1992a, Phys. Rev. Lett. **69**, 1010.
Becker-Szendy, R., *et al.*, 1993, Nucl. Inst. Meth. A **324**, 363.
Becker-Szendy, R., *et al.*, 1994, Nucl. Inst. Meth. A **326**, 1.
Berger, Ch., *et al.*, 1987, Nucl. Inst. Meth. A **262**, 463.
Berger, Ch., *et al.*, 1989a, Nucl. Phys. **B313**, 509.
Berger, Ch., *et al.*, 1989b, Phys. Lett. B **227**, 489.
Berger, Ch., *et al.*, 1990, Phys. Lett. B **245**, 305.
Berger, Ch., *et al.*, 1991, Z. Phys. C **50**, 385.
Berger, Ch., *et al.*, 1991, Phys. Lett. B **269**, 227.

Bergeson, H. E., G. L. Cassiday, and M. B. Hendricks, 1973, Phys. Rev. Lett. **31**, 66.
Bergsma, F., *et al.*, 1984, Phys. Lett. B **142**, 103.
Bernardini, P., for the MACRO collaboration, 1999, in Les Rencontres de Physique de la Vallee d'Aoste, Results and Perspectives in Particle Physics, La Thuile, Aosta Valley, Italy, Feb.-March, edited by M. Greco, p.21; hep-ex/9906019.
Bilenky, S. M., and B. Pontecorvo, 1978, Phys. Rep. **41**, 225, and references therein.
Bionta, R. M., *et al.*, 1983, Phys. Rev. Lett. **51**, 27.
Bionta, R. M., *et al.*, 1988, Phys. Rev. D **38**, 768.
Blewitt, G., *et al.*, 1985, Phys. Rev. Lett. **55**, 2114.
Boehm, F., *et al.*, 2000, Phys. Rev. Lett. **84**, 3764.
Boliev, M. M., *et al.*, 1981, Yad. Fiz. **34**, 1418 [1981, Sov. J. Nucl. Phys. **34**, 787].
Boliev, M. M., *et al.*, 1991, in *Proceedings of the Third International Workshop on Neutrino Telescopes*, Venezia, edited by Milla Baldo Ceolin, p.235.
Boliev, M. M., *et al.*, 1995, in *Proceedings of the International Cosmic Ray Conference, Rome*, Vol.1, p.686; *ibid.*, p.722.
Bonetti, S., *et al.*, 1977, Nuovo Cimento **A38**, 260.
Borodovsky, L., *et al.*, 1992, Phys. Rev. Lett. **68**, 274.
Breault, J.L., 1997, Ph.D Thesis, University of California, Irvine, unpublished.
Bugaev, E. V., and V. A. Naumov, 1989, Phys. Lett. B **232**, 391.
Butkevich, A. V., L. G. Dedenko, and I. M. Zheleznykh, 1989, Sov. J. Nucl. Phys. **50**, 90.
Casper, D. *et al.*, 1991, Phys. Rev. Lett. **66**, 2561.
Chizhov, M. V., and S. T. Petcov, 1999, Phys. Rev. Lett. **83**, 1096.
Choubey, S., and S. Goswami, 1999, hep-ph/9904257.
Circella, M., *et al.*, 1993, in *Proceedings of the XXIII International Cosmic Ray Conference*, Calgary, Canada, 1993, edited by D. A. Leahy, R. B. Hickjs, and D. Venkatesan, Vol.4, p.503.
Clark, R., *et al.*, 1997, Phys. Rev. Lett. **79**, 345.
Cleveland, B. T., *et al.*, 1998, Ap. J. **496**, 505.
Cortez, B. G., *et al.*, 1984, Phys. Rev. Lett. **52**, 1092.
Crouch, M. F., *et al.*, 1978, Phys. Rev. D **18**, 2239.
Dar, A., 1983, Phys. Rev. Lett. **51**, 227.
Daum, K., *et al.*, 1995, Z. Phys. C **66**, 417.
Dydak, F., *et al.*, 1984, Phys. Lett. **134B**, 281.
Eichten, E., *et al.*, 1984, Rev. Mod. Phys. **56**, 579.
Eskut, E., *et al.*, 1998, Phys. Lett. B **434**, 205.
Feldman, G., and R. Cousins, 1998, Phys. Rev. D **57**, 3873.
Fogli, G. L., E. Lisi, and D. Montanino, 1995, Astropart. Phys. **4**, 177.
Fogli, G. L., E. Lisi, and D. Montanino, 1997, Phys. Rev. D **56**, 4365.
Fogli, G. L., *et al.*, 1999, Phys. Rev. D **59**, 117303.
Fogli, G. L., *et al.*, 1999a, Phys. Rev. D **59**, 033001.
Fogli, G. L., *et al.*, 1999b, Phys. Rev. D **60**, 053006.
Foot, R., R. R. Volkas, and O. Yasuda, 1998, Phys. Rev. D **58**, 13006.
Fornengo, N., M. C. Gonzalez-Garcia, and J. W. F. Valle, 1999, hep-ph/9906539.
Frampton, P. H., and S. L. Glashow, 1982, Phys. Rev. D **25**, 1982.
Fukuda, Y., *et al.*, 1994, Phys. Lett. B **335**, 237.
Fukuda, Y., *et al.*, 1996a, Phys. Rev. Lett. **77**, 1683.
Fukuda, Y., *et al.*, 1996b, Phys. Lett. B **388**, 397.
Fukuda, Y., *et al.*, 1998, Phys. Rev. Lett. **81**, 1158.
Fukuda, Y., *et al.*, 1998a, Phys. Lett. B **433**, 9.
Fukuda, Y., *et al.*, 1998b, Phys. Lett. B **436**, 33.
Fukuda, Y., *et al.*, 1998c, Phys. Rev. Lett. **81**, 1562.
Fukuda, Y., *et al.*, 1999a, Phys. Rev. Lett. **82**, 2644.
Fukuda, Y., *et al.*, 1999b, Phys. Lett. B **467** 185.
Fukuda, Y., *et al.*, 2000a, draft in preparation.
Fukuda, Y., *et al.*, 2000b, draft in preparation.
Fukuda, Y., *et al.*, 2000c, draft in preparation.
Futagami, T., *et al.*, 1999, Phys. Rev. Lett. **82**, 5194.
Gabriel, T. A., *et al.*, 1989, IEEE Trans. Nucl. Sci. **36**, 14.
Gaisser, T. K., R. J. Protheroe, and T. Stanev, 1983, in *Proceedings of the 18th Int. Cosmic Ray Conf., Bangalore*, India, edited by N. Durgaprasad *et al.*, Vol. 5, p. 174.
Gaisser, T. K., *et al.*, 1983, Phys. Rev. Lett. **51**, 223.
Gaisser, T. K., *et al.*, 1996, Phys. Rev. D **54**, 5578.
Gaisser, T. K., T. Stanev and G. Barr, 1988, Phys. Rev. D **38**, 85.

Gaisser, T. K., 1998, in *New Era in Neutrino Physics, Proceedings of a Satellite Symposium after Neutrino'98 held on June 11 and 12, 1998,* Tokyo Metropolitan Univ., Japan, edited by H. Minakata and O. Yasuda, p.145.
Gaisser, T. K., and T. Stanev, 1998, Phys. Rev. D **57**, 1977.
Gell-Mann, M., P. Ramond, and R. Slansky, 1979, in *Supergravity,* edited by P. van Nieuwenhuizen and D. Z. Freedman, (North Holland, Amsterdam, 1979), p.315.
Georgi, H., and S. L. Glashow, 1974, Phys. Rev. Lett. **32**, 438.
Glück, M., E. Reya, and A. Vogt, 1995, Z. Phys. C **67**, 433.
Gonzalez-Garcia, M. C., *et al.*, 1999, Phys. Rev. Lett. **82**, 3202.
Gribov, V., and B. Pontecorvo, 1969, Phys. Lett. **28B**, 463.
Haines, T. J., *et al.*, 1986, Phys. Rev. Lett. **57**, 1986.
Hall, L. J. and H. Murayama, 1998, Phys. Lett. B, **436** 323.
Hampel, W., *et al.*, 1999, Phys. Lett. B, **447** 127.
Hänssget, K. and J. Ranft, 1986, Comput. Phys. **39**, 37.
Hatakeyama, S., *et al.*, 1998, Phys. Rev. Lett. **81**, 2016.
Hayato, Y., *et al.*, 1999, Phys. Rev. Lett. **83**, 1529.
Hidaka, K., M. Honda, and S. Midorikawa, 1988, Phys. Rev. Lett. **61**, 1537.
Hillas, A. M., 1972, *Cosmic Rays,* Pergamon Press, Part 1, Chapter 2.
Hirata, K. S., *et al.*, 1988, Phys. Lett. B **205**, 416.
Hirata, K. S., *et al.*, 1989, Phys. Lett. B **220**, 308.
Hirata, K. S., *et al.*, 1992, Phys. Lett. B **280**, 146.
Honda, M., *et al.*, 1990, Phys. Lett. B **248**, 19
Honda, M., *et al.*, 1995, Phys. Rev. D **52**, 4985.
Honda, M., K. Kasahara, and S. Midorikawa, 1999, in *Proceedings of the 26th International Cosmic Ray Conference,* Utah, USA, Aug. 1999, HE.4.1.09, and private communication with M. Honda.
Jannakos, T. E., *et al.*, 1999, hep-ex/9908043.
Johnson, T. H., 1933a, Phys. Rev. **43**, 307.
Johnson, T. H., 1933b, Phys. Rev. **43**, 381.
Johnson, T. H., 1935, Phys. Rev. **48**, 287.
Kajita, T., *et al.*, 1986, J. Phys. Soc. Jpn. **55**, 711.
Kajita, T., for the Kamiokande collaboration, 1990, in *Proceedings of the 25th International Conference on High Energy Physics,* Singapore, edited by K. K. Phua and Y. Yamaguchi, p.685.
Karle, A., for the AMANDA collaboration, 1999, in *Proceedings of the 26th International Cosmic Ray Conference,* Utah, edited by D. Kieda, M. Salamom and B. Dingus, Vol.2, p.221.
Kasahara, K., *et al.*, 1979, in *Proceedings of the 16th International Cosmic Ray Conference,* Kyoto, Japan, 1979, Vol.13, p.70.
Kasuga, S., *et al.*, 1996, Phys. Lett. B **374**, 238.
Krishnaswamy, M. R., *et al.*, 1971, Proc. Roy. Soc. Lond. A. **323**, 489.
Krishnaswamy, M. R., *et al.*, 1981, Phys. Lett. **106B**, 339.
Krishnaswamy, M. R., *et al.*, 1982, Phys. Lett. **115B**, 349.
Krishnaswamy, M. R., *et al.*, 1986, Nuovo Cimento **9C**, 167.
Langacker, P., 1981, Phys. Rep. **72**, 185.
Lanou Jr., R. E., 1998, in Proceedings of the XVIII International Conference on Neutrino Physics and Astrophysics, Takayama, Japan, June 1998, edited by Y. Suzuki and Y. Totsuka, p.55.
Learned, J. G., S. Pakvasa, and T. J. Weiler, 1988, Phys. Lett. B **207**, 79.
Learned, J. G., S. Pakvasa, and J. L. Stone, 1998, Phys. Lett. B **435**, 131.
Lee, H., and Y. S. Koh, 1990, Nuovo Cimento B **105**, 883.
Lipari, P., 1993, Astropart. Phys. **1**, 195.
Lipari, P., M. Lusignoli, and F. Sartogo, 1995, Phys. Rev. Lett. **74**, 4384.
Lipari, P., T. Stanev, and T. K. Gaisser, 1998, Phys. Rev. D **58**, 073003.
Lipari, P., and M. Lusignoli, 1998, Phys. Rev. D **57**, 3842.
Lipari, P., and M. Lusignoli, 1998a, Phys. Rev. D **58**, 073005.
Lipari, P., and M. Lusignoli, 1999, Phys. Rev. D **60**, 013003.
Lipari, P., 2000a, hep-ph/0002282.
Lipari, P., 2000b, hep-ph/0003013.
Liu, Q.Y., S. P. Mikheyev, and A. Yu. Smirnov, 1998, Phys. Lett. B, **440** 319.
Llewellyn Smith, C. H, 1972, Phys. Rep. **3**, 261.
LoSecco, J. M., *et al.*, 1985, Phys. Rev. Lett. **54**, 2299.
Maki, Z., M. Nakagawa, and S. Sakata, 1962, Prog. Theo. Phys. **28**, 870.
Mann, W. A., T. Kafka and W. Leeson, 1992, Phys. Lett. B **291**, 200.
Mann, A., 1999, talk presented at *the XIX International Symposium Lepton and Photon Interactions at High Energies,* Aug. 1999, Stanford University; to be published in the proceedings; hep-ex/9912007.

McDonald, A. B., for the SNO collaboration, 1998, in Proceedings of the XVIII International Conference on Neutrino Physics and Astrophysics, Takayama, Japan, June 1998, edited by Y. Suzuki and Y. Totsuka, p.43.
McGrew, C., *et al.*, 1999, Phys. Rev. D **59**, 052004.
Meier, C., and T. Ohlsson, 1999, hep-ph/9910270.
Mikheyev, S. P., and A. Yu. Smirnov, 1985, Sov. J. Nucl. Phys. **42**, 1441.
Mikheyev, S. P. and A. Yu. Smirnov, 1986, Nuovo Cimento **C9**, 17.
Nakagawa, M., *et al.*, 1963, Prog. Theo. Phys. **30**, 727.
Nakahata, M., *et al.*, 1986, J. Phys. Soc. Jpn. **55**, 3786.
Nakamura, K., *et al.*, 1994, in *Physics and Astrophysics of Neutrinos*, edited by M. Fukugita and A. Suzuki, (Springer-Verlag, Tokyo), p.249.
Nilsson-Almqvist, B. and E. Stenlund, 1987, Comput. Commun. **43**, 387.
Nishikawa, K., 1998, in Proceedings of the XVIII International Conference on Neutrino Physics and Astrophysics, Takayama, Japan, June 1998, edited by Y. Suzuki and Y. Totsuka, p.198.
Oberauer, L., 1998, in Proceedings of the XVIII International Conference on Neutrino Physics and Astrophysics, Takayama, Japan, June 1998, edited by Y. Suzuki and Y. Totsuka, p.48.
Oset, E., *et al.*, 1988, Nucl. Phys. A **484**, 557.
Osborne, J. L., S. S. Said and A. W. Wolfendale, 1965, Proc. Phys. Soc. **86**, 93.
Pakvasa, S., 1980, in *Proceedings of the 1980 International Dumand Symposium*, July-Aug., 1980, Hawaii, U.S.A., edited by V. J. Stenger, Vol. II, p.45.
Pantaleone, J., 1998, Phys. Rev. Lett. **81**, 5060.
Park, H. S., *et al.*, 1985, Phys. Rev. Lett. **54**, 22.
Particle Data Group, 1998, Eur. Phys. J. C **3**, 320.
Pati, C. J., and A. Salam, 1973, Phys. Rev. Lett. **31**, 661.
Peres, O. L. G., and A. Yu. Smirnov, 1999, Phys. Lett. B **456**, 204.
Perkins, D. H., 1984, Ann. Rev. Nucl. Part. Sci. **34**, 1.
Perkins, D. H., 1994, Astropart. Phys. **2**, 249.
Phillips, T. J., 1989, Phys. Lett. B **224**, 348.
Picchi, P. and F. Pietropaolo, 1998, in Proceedings of the XVIII International Conference on Neutrino Physics and Astrophysics, Takayama, Japan, June 1998, edited by Y. Suzuki and Y. Totsuka, p.187.
Pontecorvo, B., 1957, Zh. Eksp. Teor. Fiz. **33** 549 [1958, JETP **6**, 429].
Pontecorvo, B., 1967, Zh. Eksp. Teor. Fiz. **53** 1717 [1968, Sov. Phys. JETP **26**, 984].
Rein, D., and L. M. Sehgal, 1981, Ann. of Phys. **133**, 79.
Rein, D., and L. M. Sehgal, 1983, Nucl. Phys. **B223**, 29.
Reines, F., *et al.*, 1965, Phys. Rev. Lett. **15**, 429.
Reines, F., *et al.*, 1971, Phys. Rev. D **4**, 80.
Romosan, A., *et al.*, 1997, Phys. Rev. Lett. **78**, 2912.
Rossi, B., 1964, 'Cosmic Rays', McGraw Hill, and references therein.
Ryazhskaya, O. G., 1994, JETP Lett. **60**, 617.
Ryazhskaya, O. G., 1995, JETP Lett. **61**, 237.
Sakai, T., and T. Teshima, 1999, Phys. Rev. Lett. **61**, 2522.
Seidel, S., *et al.*, 1988, Phys. Rev. Lett. **61**, 2522.
Shiozawa, M., *et al.*, 1998, Phys. Rev. Lett. **81**, 3319.
Sjöstrand, T. and M. Bengtsson, 1987, Comput. Commun. **43**, 367.
Sjöstrand, T., 1994, CERN-TH-7112-93.
Spurio, M., for the MACRO collaboration, 1999, to be published in Proceedings of Sixth Topical Seminar on Neutrino and Astro-Particle Physics, San Miniato, Italy, May 1999; hep-ex/9908066.
Steidl, M., for the KARMEN collaboration, 1999, in Les Rencontres de Physique de la Vallee d'Aoste, Results and Perspectives in Particle Physics, La Thuile, Aosta Valley, Italy, Feb.-March, edited by M. Greco, p.35.
Tam, A. C., and E. C. M. Young, 1969, in *Proceedings of the 11th Int. Conf. on Cosmic Rays*, Budapest, Acta. Phys. Hungarica **29**, Suppl. 4, 1970, p.307.
Tserkovnyak, Y., *et al.*, 1999, hep-ph/9907450.
Volkova, L. V., 1980, Sov. J. Nucl. Phys. **31**, 784.
Volkova, L. V., 1988, private communication; see also (Volkova, 1980).
Webber, W. R., and J. A. Lezniak, 1974, Astrophys. Space Sci. **30**, 361.
Wojcicki, S. G., 1998, in Proceedings of the XVIII International Conference on Neutrino Physics and Astrophysics, Takayama, Japan, June 1998, edited by Y. Suzuki and Y. Totsuka, p.182.
Wolfenstein, L., 1978, Phys. Rev. D **17**, 2369.
Yanagida, T., 1979, in *Proceedings of the Workshop on the Unified Theory and Baryon Number in the Universe*, edited by O. Sawada and A. Sugamoto (KEK report 79-18, 1979), p.95.
Yasuda, O., 1998, Phys. Rev. D **58**, 091301.

Experiment	Status of[a] experiment	Detection technique	Type of events	Fiducial mass	Total exposure	Number of events
Baksan	running	liquid scintillator	up-through-μ	—	10.55 yr	424
NUSEX	finished	gas counter-iron plate	FC	0.13 kt	0.74 kt·yr	50
Frejus	finished	gas counter-iron plate	FC	0.7 kt	2.0 kt·yr	158
			PC	0.7 kt	2.0 kt·yr	58
Kamiokande	finished	water-Cherenkov	FC	1.04~1.35 kt	7.7~8.2 kt·yr	885
			PC	1.04 kt	6.0 kt·yr	118
			up-through-μ	—	6.7 yr	372
IMB	finished	water-Cherenkov	FC	3.3 kt	7.7 kt·yr	935
			up-through-μ	—	3.6 yr	532
			up-stopping-μ	—	3.6 yr	85
Soudan-2	running	gas counter-iron plate	FC	0.77 kt	3.9 kt·yr	371
MACRO	running	liquid scintillator + gas counter	up-through-μ	—	5.9 yr[b]	607
Super-Kamiokande	running	water-Cherenkov	FC	22.5 kt	61 kt·yr	7940
			PC	22.5 kt	61 kt·yr	563
			up-through-μ	—	2.94 yr	1187
			up-stopping-μ	—	2.88 yr	265

(a) As of 1999.
(b) Detector exposure with the full detector is 4.1 yr.

TABLE I. Summary of atmospheric neutrino experiments which observed fully-contained (FC), partially-contained (PC), upward stopping muon, and upward through-going muon events.

Type of events	CC ν_e	CC ν_μ	NC
FC, sub-GeV			
1-ring, e-like	87.1%	3.1%	9.8%
1-ring, μ-like	0.4%	95.4%	4.2%
multi-ring	22.0%	42.4%	35.6%
FC, multi-GeV			
1-ring, e-like	83.6%	7.3%	9.1%
1-ring, μ-like	0.2%	99.5%	0.3%
multi-ring	32.9%	52.6%	14.4%
PC	1.9%	97.1%	0.9%
Upward stopping muons	$\ll$1%	$\gg$99%	$\ll$1%
Upward through-going muons	$\ll$1%	$\gg$99%	$\ll$1%

TABLE II. Estimated fraction of CC ν_e, CC ν_μ and NC events for each event type in Super-Kamiokande (Fukuda *et al.*, 1998a, 1998b, 1999a, 1999b, 2000a).

Source	sub-GeV	Multi-GeV
Predicted (ν_μ/ν_e) flux ratio	5%	5%
Spectrum index of the neutrino fluxes	0.6%	1.6%
Data reduction	$\ll$1%	3%
μ/e separation	2%	3%
1-ring/>2-ring separation	3%	6%
Vertex position uncertainty	0.6%	2.4%
Absolute energy calibration	1.0%	4.1%
Background contamination (cosmic ray μ)	<0.1%	<0.2%
Background contamination (neutron)	<0.1%	<0.2%
Background contamination (PMT flashing)	<0.5%	<0.1%
FC/PC separation	<0.1%	0.5%
CC cross section	3.6%	4.3%
NC cross section	3%	4%
Simulation of hadron interactions in water	0.5%	1%
Stat. error of MC	0.7%	1.4%
Total	7.8%	12%

TABLE III. Summary of the systematic errors in the $(\mu/e)_{Data}/(\mu/e)_{MC}$ flux ratio measurement in Super-Kamiokande for the sub- and multi-GeV samples (Fukuda *et al.*, 1998a, 1998b, 2000a).

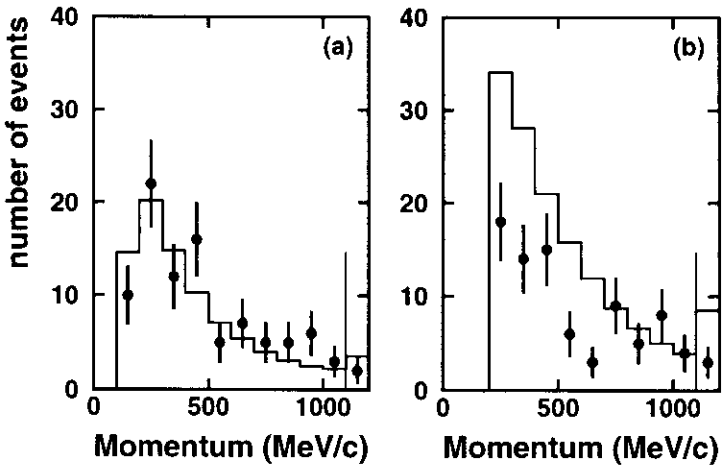

FIG. 1. Momentum distributions for (a) e-like and (b) μ-like events observed in Kamiokande in 1988 (Hirata *et al.*, 1988). The histograms are the predictions based on the flux calculation of (Gaisser *et al.*, 1988).

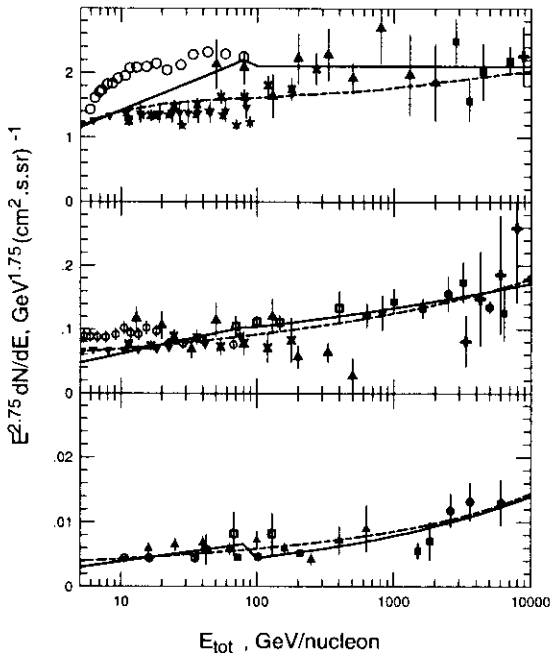

FIG. 2. Spectra of proton (top), helium (middle) and CNO nuclei (bottom). Open circles, inverted-filled triangles, × and stars show data obtained by various magnetic spectrometers. Higher energy data in this energy range were obtained by calorimeter experiments. Dashed curves show the primary cosmic-ray spectra assumed in (Agrawal *et al.*, 1996) and solid curves those in (Honda *et al.*, 1995). This figure is taken from (Gaisser, 1998). See (Gaisser, 1998) for the references of the cosmic ray data.

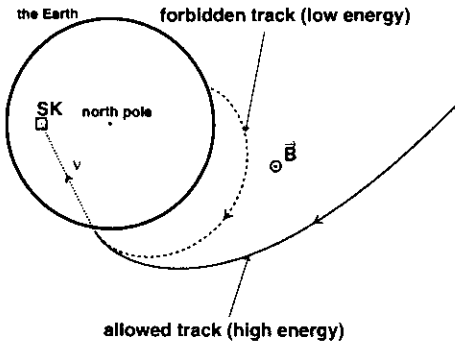

FIG. 3. Typical allowed and forbidden tracks of incident cosmic rays. The curved line shows the allowed trajectory of a cosmic ray which has a rigidity larger than the cutoff rigidity and the dotted curved line shows a forbidden trajectory. 'SK' represents an atmospheric neutrino detector.

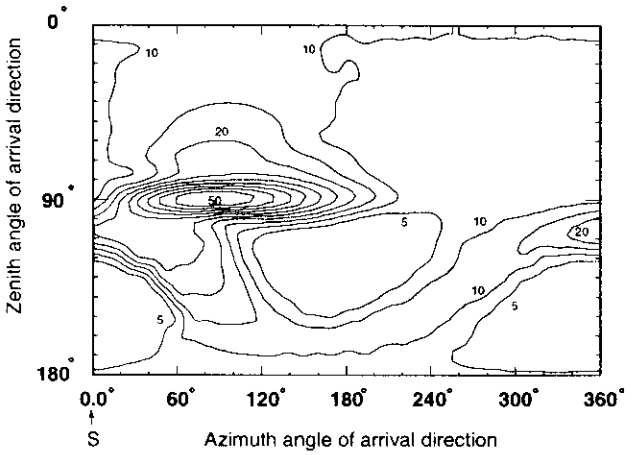

FIG. 4. The contour map of calculated cutoff rigidity (GeV/cZ) for the neutrino arrival directions at Kamioka (Honda *et al.*, 1995). Azimuthal angles of 0°, 90°, 180° and 270° show directions to the south, east, north, and west of the detector, respectively. Zenith angle 0°(180°) corresponds to a direction directly overhead (below).

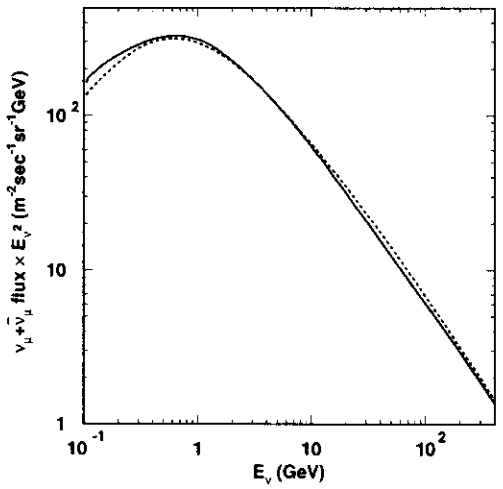

FIG. 5. The calculated flux of atmospheric $(\nu_\mu + \overline{\nu}_\mu)$ by Honda *et al.*, (1995) (solid line), and Agrawal *et al.*, (1996) (dashed line). The fluxes are integrated over solid angle and multiplied by E_ν^2.

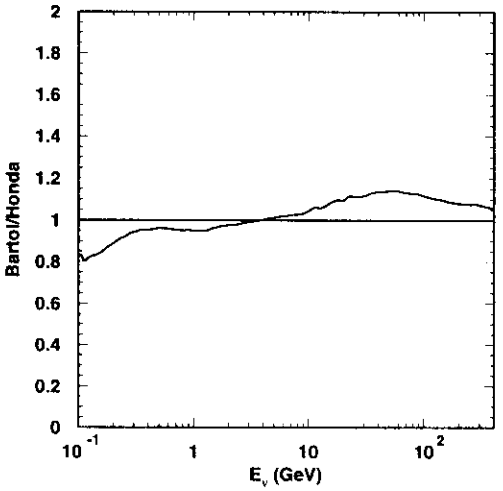

FIG. 6. Comparison of the absolute values of the calculated atmospheric neutrino fluxes by Honda *et al.* (1995) and Agrawal *et al.* (1996). "Bartol" represents the flux calculated by Agrawal *et al.* (1996).

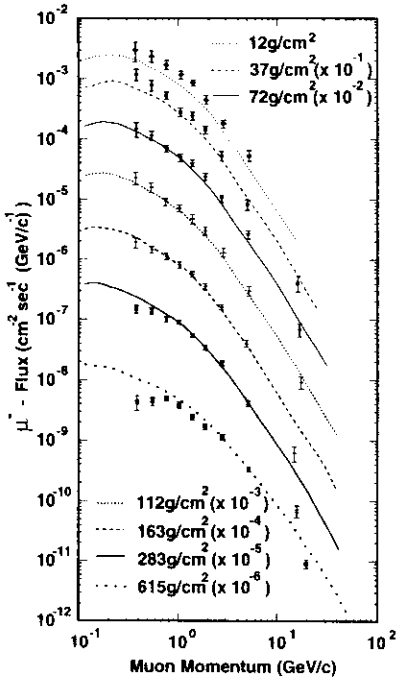

FIG. 7. Comparison of the calculated μ^- flux by Honda *et al.* (1995) and data from the MASS experiment (Circella *et al.*, 1993) at various altitudes.

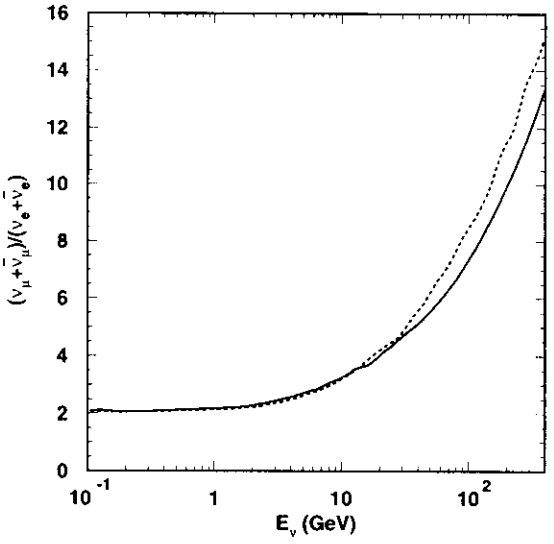

FIG. 8. The calculated $(\nu_\mu + \overline{\nu}_\mu)/(\nu_e + \overline{\nu}_e)$ flux ratio by Honda *et al.* (1995) (solid line), and Agrawal *et al.* (1996) (dashed line).

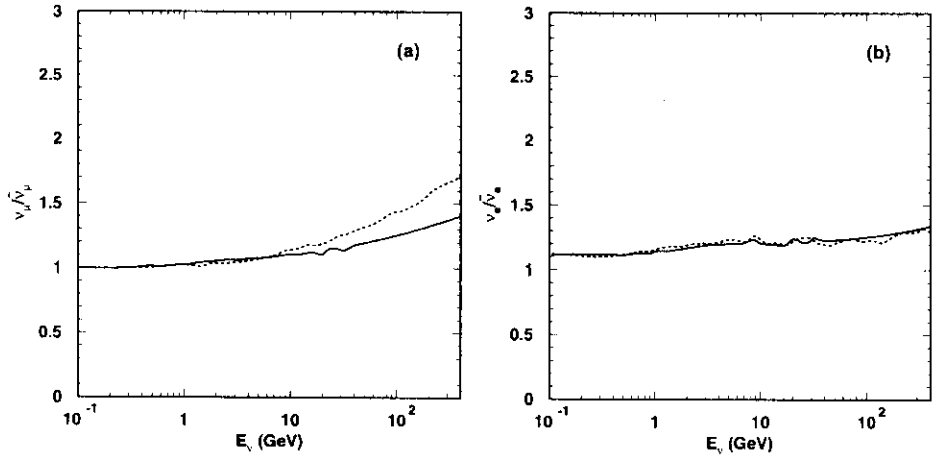

FIG. 9. The calculated (a) $\nu_\mu/\overline{\nu}_\mu$ and (b) $\nu_e/\overline{\nu}_e$ flux ratios by Honda *et al.* (1995) (solid lines), and Agrawal *et al.* (1996) (dashed lines).

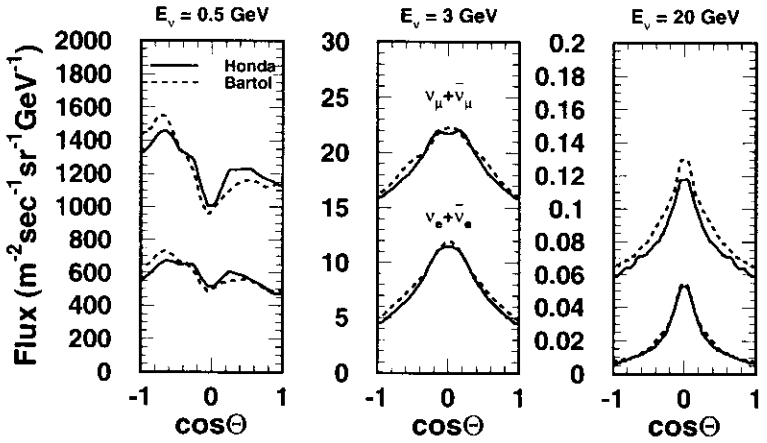

FIG. 10. The calculated zenith angle distributions of the atmospheric neutrino fluxes for several neutrino energies by Honda *et al.* (1995) (solid lines), and Agrawal *et al.* (1996) (dashed lines).

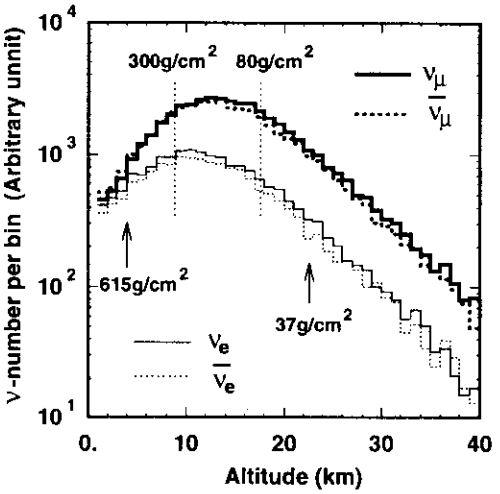

FIG. 11. The calculated distribution of the production heights of atmospheric neutrinos for E_ν >0.4 GeV by Honda *et al.* (1995).

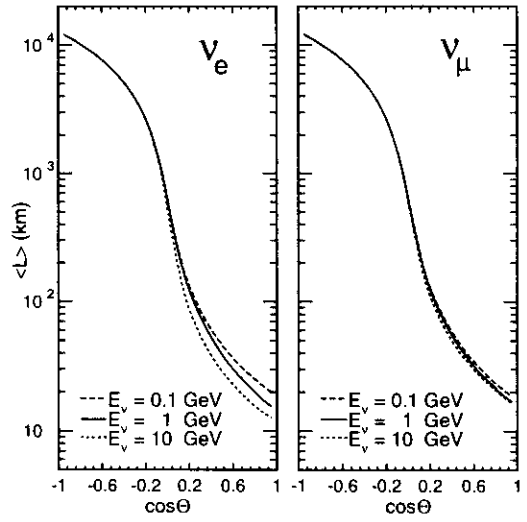

FIG. 12. The mean flight length of atmospheric neutrinos as a function of the zenith angle for ν_e (left) and ν_μ (right) and for three neutrino energies. This figure was made based on Gaisser and Stanev (1998).

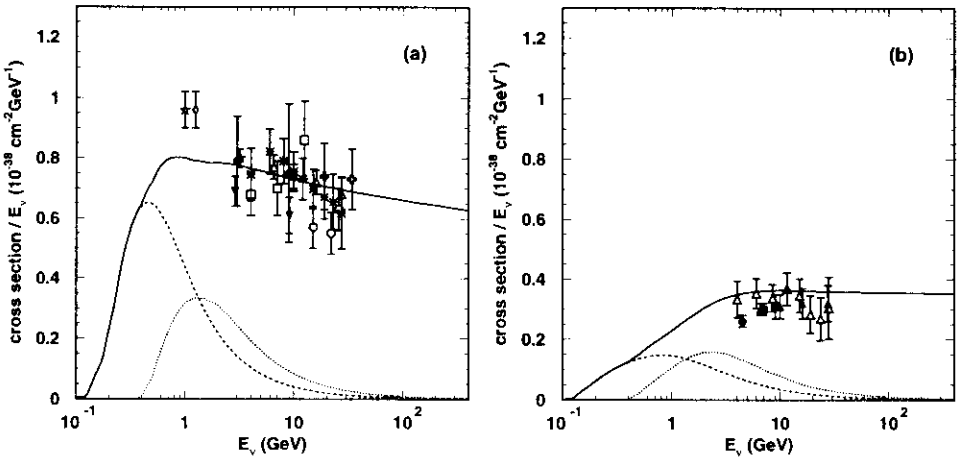

FIG. 13. (Total cross section / E_ν) for CC (a) neutrino interactions and (b) anti-neutrino interactions. The calculated cross sections (solid lines) are compared with experimental data from various accelerator experiments (see Anikeev *et al.*, 1996, and references therein). Also shown are the (cross section / E_ν) of the quasi-elastic (dashed lines) and single-pion production (dotted lines) interactions.

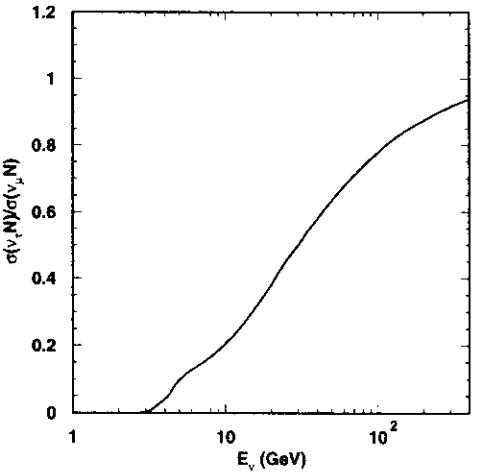

FIG. 14. Ratio of the total cross section, $\sigma(\nu_\tau N)/\sigma(\nu_\mu N)$, as a function of neutrino energy. The Fermi motion of the target nucleon is taken into account.

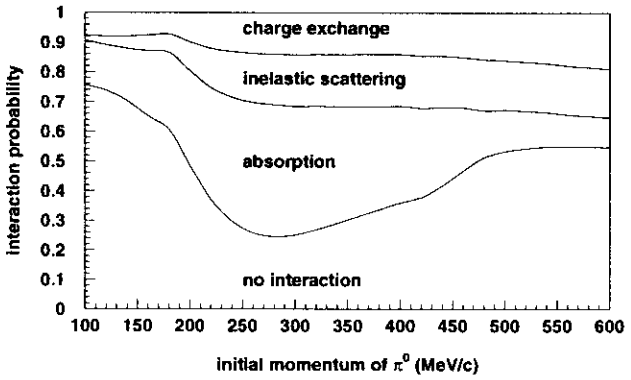

FIG. 15. Calculated probability of π^0 interactions in a ^{16}O nucleus. Initial positions of the π^0 are randomly selected within the nucleus according to the estimated nuclear density.

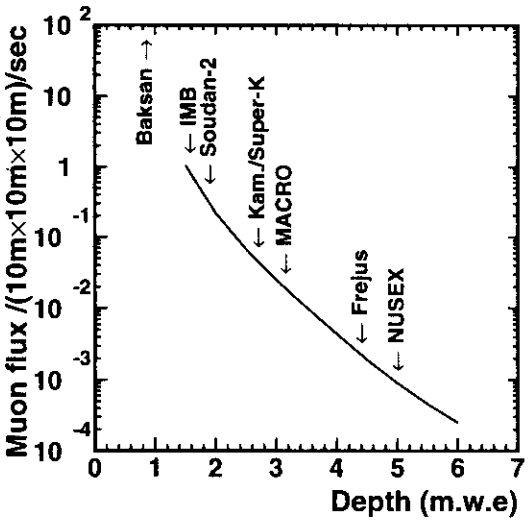

FIG. 16. Depth of the detectors and the calculated cosmic-ray muon rate (solid line). This figure is a modified version of (Perkins, 1984).

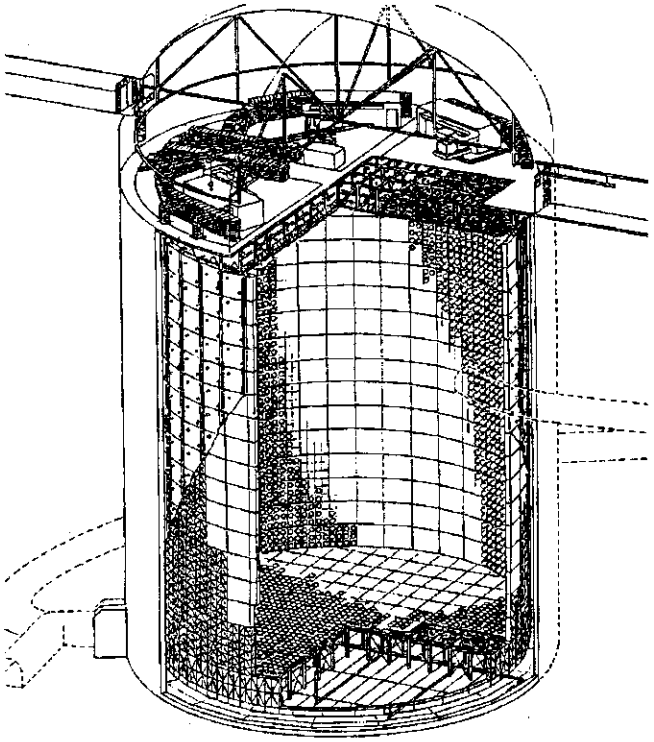

FIG. 17. The Super-Kamiokande detector. The inner water Cherenkov detector of 32,000 ton is surrounded by a 4π water Cherenkov outer-detector (anti-counter). The total weight of the detector is 50,000 tons, the height is 42 meters and the diameter is 39 meters.

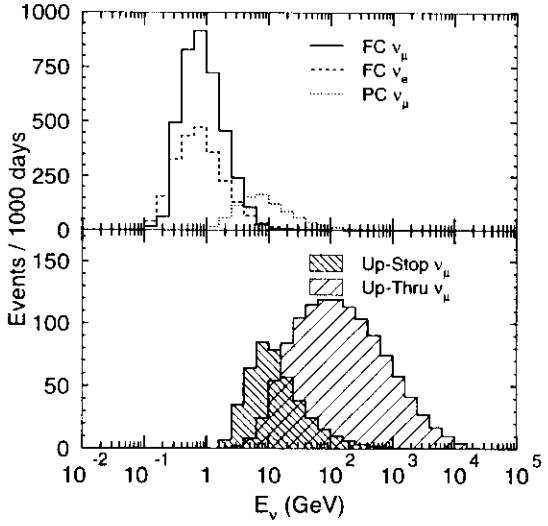

FIG. 18. Distributions of the estimated neutrino energies for various types of neutrino events in Super-Kamiokande. The number of events is normalized to 1000 days of exposure of the Super-Kamiokande detector. The distributions of neutrino energies in other detectors should be similar to these.

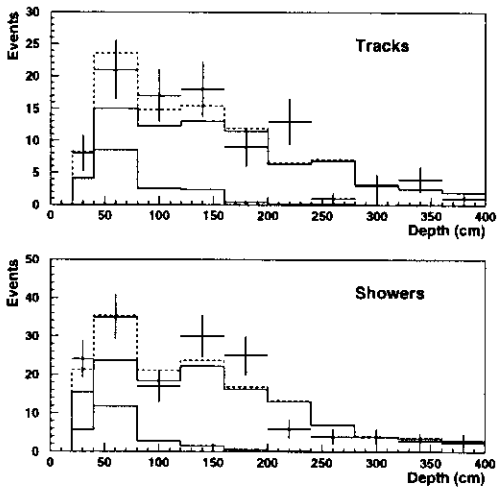

FIG. 19. Distributions of the minimum distance between the event vertex and the detector exterior (excluding the detector floor) in Soudan-2 (Allison *et al.*, 1999). Crosses show the "gold" events which have no anti-counter hits. The shaded histograms show the distributions of events with anti-counter hits. Open histograms show the atmospheric neutrino MC distributions. The shaded and open histograms are normalized to the fitted background and neutrino events present in the "gold" sample. The sums of these two histograms are shown by dashed histograms, which show the best fit to the "gold" data.

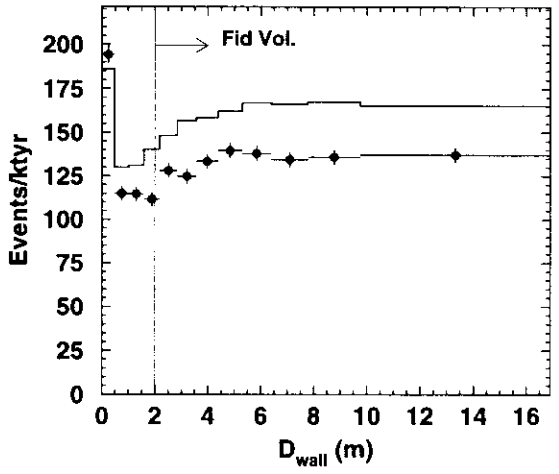

FIG. 20. Distribution of the minimum distance between the vertex position and the PMT plane of the inner-detector of Super-Kamiokande (D_{wall}). Black circles with error bars show the FC data and the histogram shows the atmospheric neutrino MC without neutrino oscillations. The excess of the (Monte Carlo) events at the bin nearest to the PMT plane ($D_{wall} \simeq 0$) is due to a constraint in the vertex reconstruction: the reconstructed vertex position was constrained to be inside the inner-detector, and therefore events which had the best-fit vertex position outside of the inner-detector were reconstructed as $D_{wall} \simeq 0$.

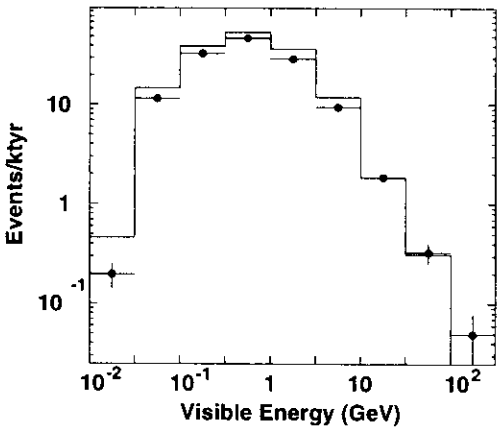

FIG. 21. Distribution of visible energy (E_{vis}) for FC events observed in Super-Kamiokande. Black circles with error bars show the data and the histogram shows the atmospheric neutrino MC without neutrino oscillations. Visible energy is defined to be the energy of an electron which would produce the observed amount of Cherenkov light.

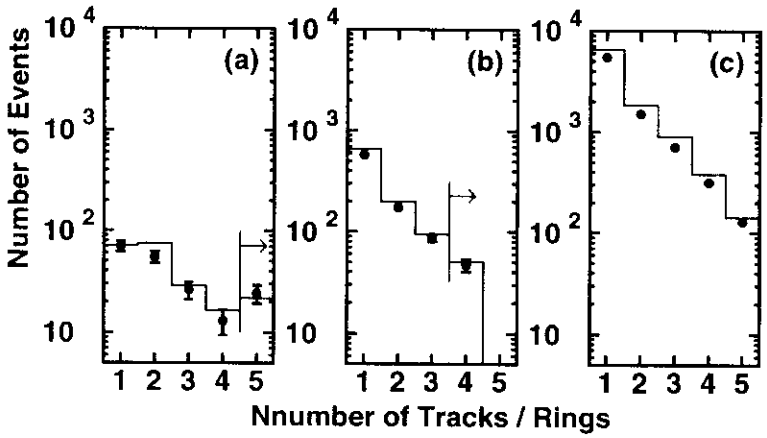

FIG. 22. (a) shows the distribution of the number of charged tracks observed in the Frejus experiment (Berger *et al.*, 1989b). (b) and (c) show the distributions of the number of Cherenkov rings observed in Kamiokande (Fukuda *et al.*, 1994) and Super-Kamiokande (Fukuda *et al.*, 2000a), respectively. The black circles with error bars show the data and the histograms show the Monte Carlo predictions. The arrows refer to bins which include all higher track (or Cherenkov ring) multiplicity events.

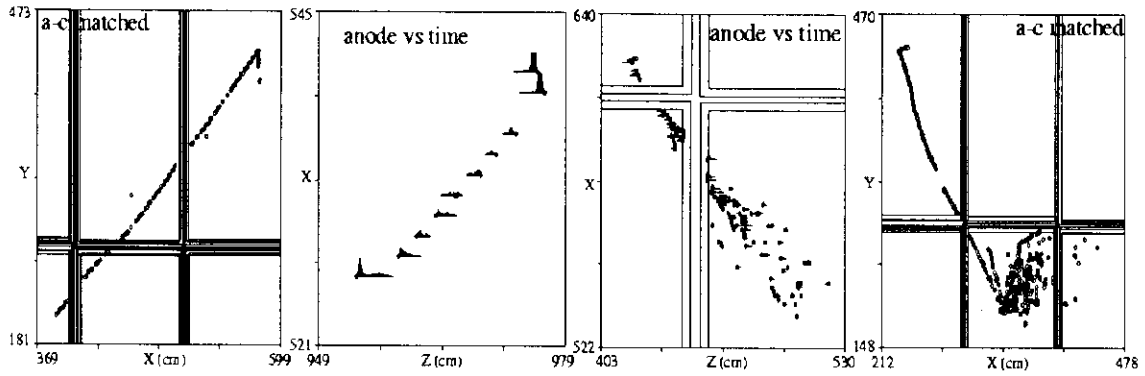

FIG. 23. From left to right: two track-plus-recoil events, a single shower event, and a CC ν_μ multi-prong event observed in the Soudan-2 detector (Mann, 1999).

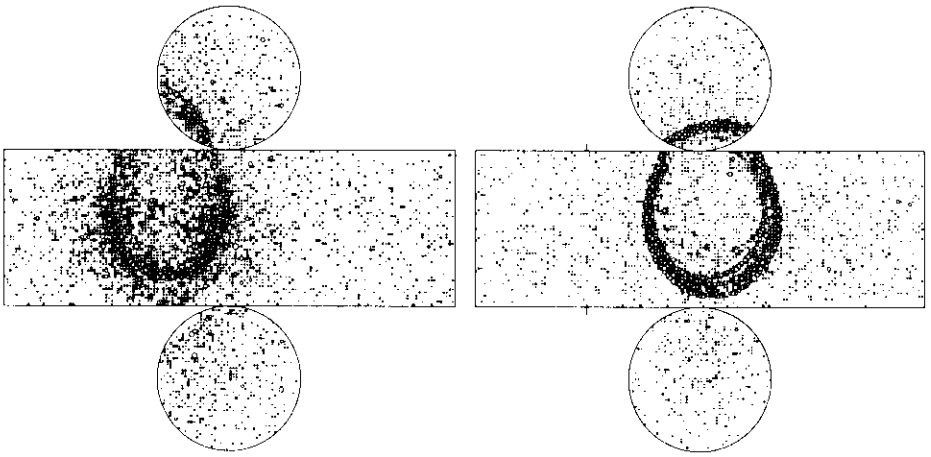

FIG. 24. An e-like (left) and a μ-like (right) event observed in the Super-Kamiokande detector.

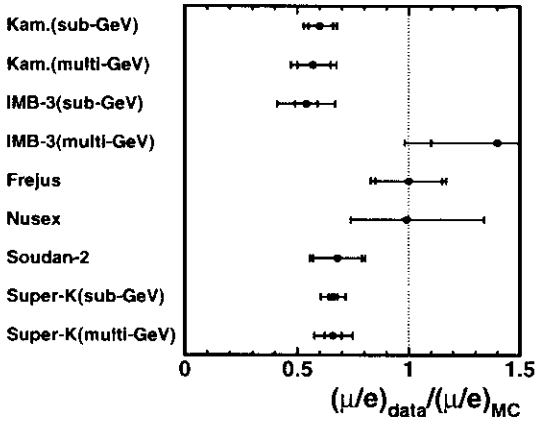

FIG. 25. Summary of the $(\mu/e)_{Data}/(\mu/e)_{MC}$ flux ratio measurements. Inner error bars show the statistical error and the outer error bars show the total error which is defined to be a quadratic sum of the statistical and systematic errors. The uncertainty in the predicted flux ratio is included in the systematic error. Data are from Kamiokande (Fukuda *et al.*, 1994), IMB-3 (Becker-Szendy *et al.*, 1992, Clark *et al.*, 1997), Frejus (Daum *et al.*, 1995), NUSEX (Aglietta *et al.*, 1989), Soudan-2 (Allison *et al*, 1999, Mann, 1999), Super-Kamiokande (Fukuda *et al.*, 2000a).

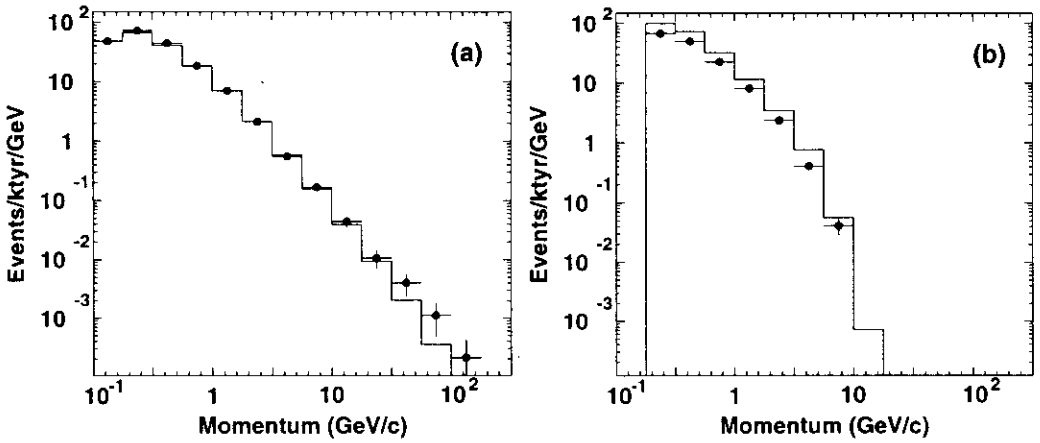

FIG. 26. The momentum spectra of the single-ring (a) e-like events and (b) μ-like events observed in Super-Kamiokande. The cut-off of the momentum spectrum for μ-like events near 10 GeV/c is due to the requirement of full containment.

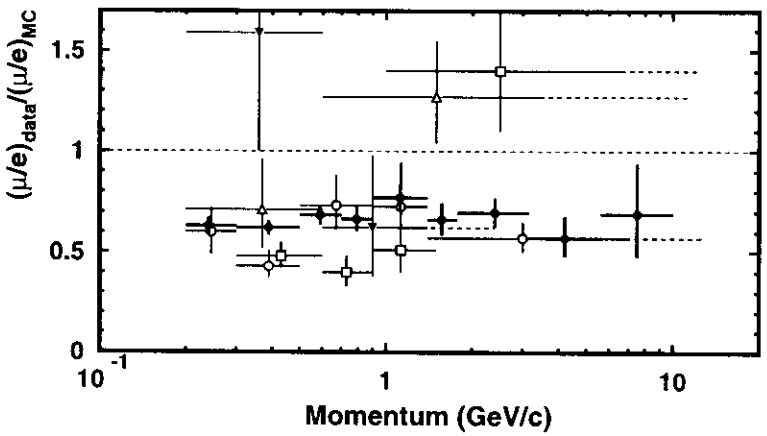

FIG. 27. Momentum dependence of $(\mu/e)_{Data}/(\mu/e)_{MC}$ from Super-Kamiokande (black circles, Fukuda *et al.*, 2000a), Kamiokande (blank circles, Fukuda *et al.*, 1994), IMB-3 (squares, Becker-Szendy *et al.*, 1992; Clark *et al.*, 1997), Frejus (blank-triangles, Berger *et al.*, 1989b), and NUSEX (black-triangles, Aglietta *et al.*, 1989). The vertical error bars show the statistical errors only. The dashed extensions of the horizontal error bars refer to bins which include all higher energy events.

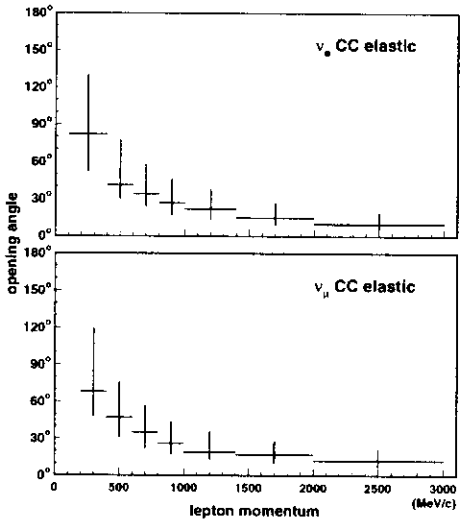

FIG. 28. Estimated correlation angle between neutrinos and leptons produced by neutrino interactions for the atmospheric neutrino fluxes.

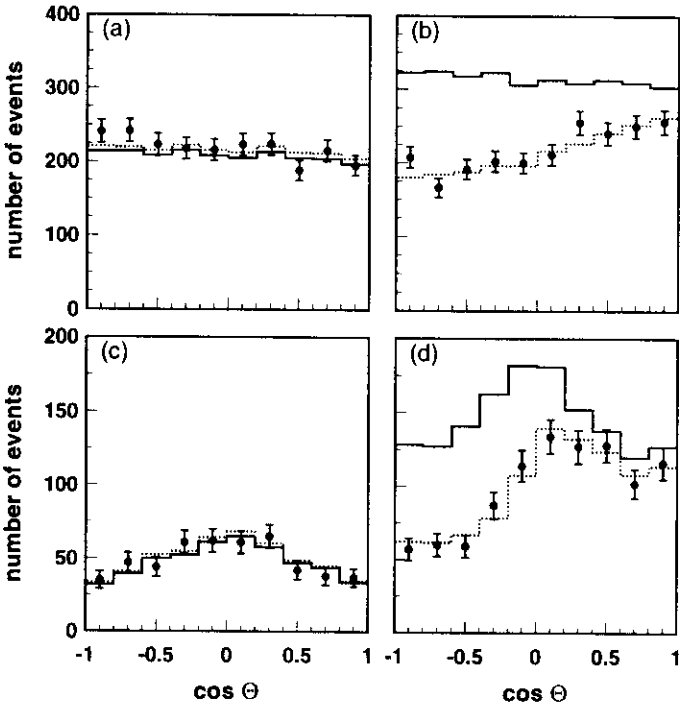

FIG. 29. Zenith angle distributions observed in Super-Kamiokande based on 61 kton·yr data for (a) sub-GeV e-like, (b) sub-GeV μ-like, (c) multi-GeV e-like, and (d) multi-GeV μ-like events. PC events are included in (d). CosΘ =1(−1) means down-going (up-going). The solid histograms show the Monte Carlo prediction without neutrino oscillations. The dashed histograms show the prediction with neutrino oscillations (Δm^2 =2.8×10^{-3} eV^2, $\sin^2 2\theta$ =1.0). In the oscillated Monte Carlo, the absolute normalization was adjusted to give the best fit to the data.

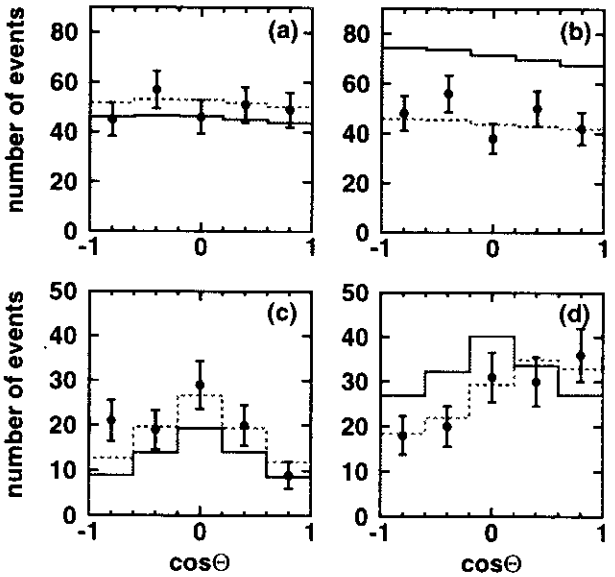

FIG. 30. Zenith angle distributions observed in Kamiokande (Fukuda *et al.*, 1994) for (a) sub-GeV e-like, (b) sub-GeV μ-like, (c) multi-GeV e-like, and (d) multi-GeV μ-like events. PC events are included in (d). CosΘ =1(−1) means down-going (up-going). The solid histograms show the Monte Carlo prediction without neutrino oscillations. The dashed histograms show the prediction with neutrino oscillations (Δm^2 =1.6×10^{-2} eV^2, $\sin^2 2\theta$ =1.0). In the oscillated Monte Carlo, the absolute normalization was adjusted to give the best fit to the data.

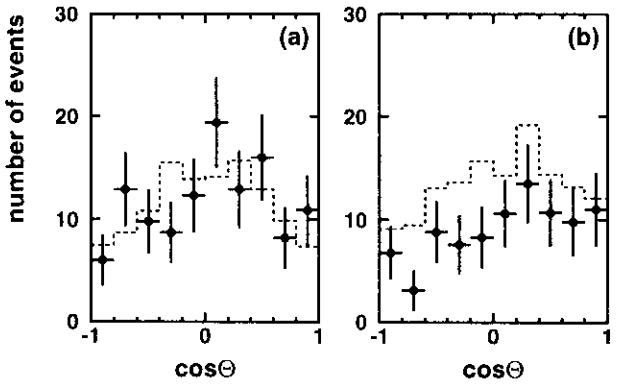

FIG. 31. Zenith angle distributions observed in Soudan-2 for the (a) CC ν_e and (b) CC ν_μ samples (Mann, 1999). The histograms show the Monte Carlo prediction without neutrino oscillations.

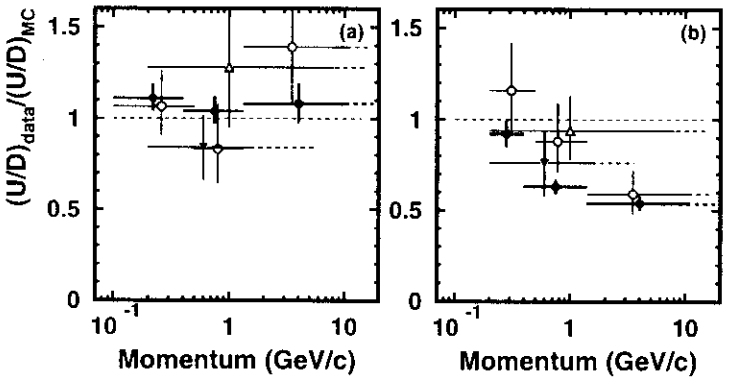

FIG. 32. Summary of $(U/D)_{Data}/(U/D)_{MC}$ as a function of lepton momentum from various experiments for (a) e-like events and (b) μ-like events. Black circles show the Super-Kamiokande data (Fukuda *et al.*, 1998c, 2000a), blank circles the Kamiokande data (Fukuda *et al.*, 1994), black triangles the Soudan-2 data (Mann, 1999), and the blank triangles the Frejus data (Berger *et al.*, 1989b). The vertical error bars show the statistical errors only. The dashed extensions of the horizontal error bars refer to bins which include all higher energy events.

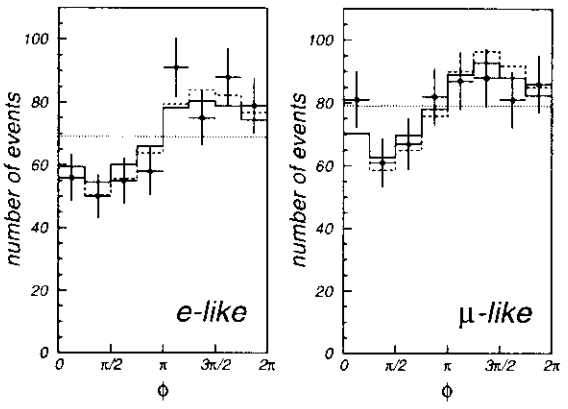

FIG. 33. Azimuthal angle distribution for e-like and μ-like events observed in Super-Kamiokande (Futagami *et al.*, 1999). The crosses represent the data, the solid and dashed histograms show the Monte Carlo prediction based on the flux of (Honda *et al.*, 1990, 1995) and (Agrawal *et al.*, 1996; Lipari, Stanev and Gaisser, 1998), respectively. Data are shown with statistical errors. The Monte Carlo is normalized to the total number of data events. ϕ represents the azimuthal angle. $\phi = 0$, $\pi/2$, π and $3\pi/2$ correspond to particles going to north, west, south and east, respectively.

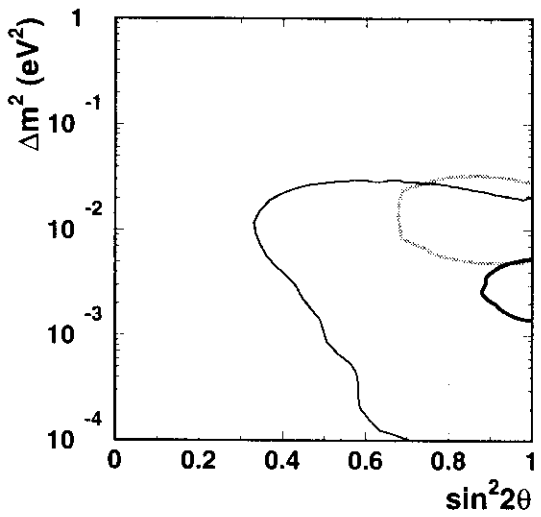

FIG. 34. 90% C.L. allowed regions of the $\nu_\mu \rightarrow \nu_\tau$ neutrino oscillation parameters by the analyses of contained events from Super-Kamiokande (thick-black line, Fukuda *et al.*, 1998c, 2000a), Kamiokande (thick-gray line, Fukuda *et al.*, 1994) and Soudan-2 (thin-black line, Mann, 1999). The allowed regions correspond to the insides of each curve.

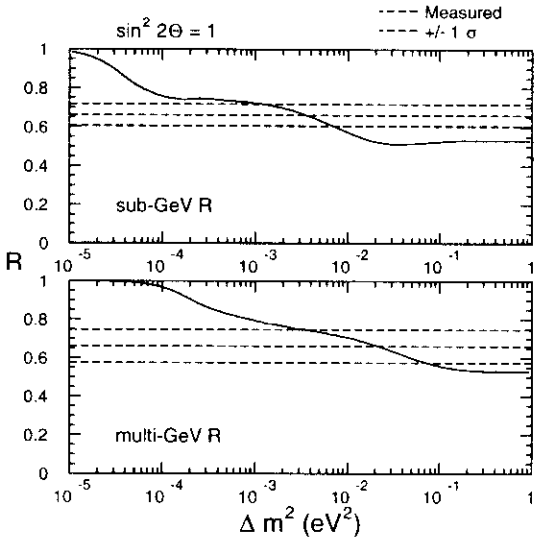

FIG. 35. The expected $(\mu/e)_{Data}/(\mu/e)_{MC}$ values for sub- and multi-GeV energy ranges are shown as a function of Δm^2 (solid curves). Also shown are the observed $(\mu/e)_{Data}/(\mu/e)_{MC}$ values with their errors (dashed lines). $R \equiv (\mu/e)_{Data}/(\mu/e)_{MC}$.

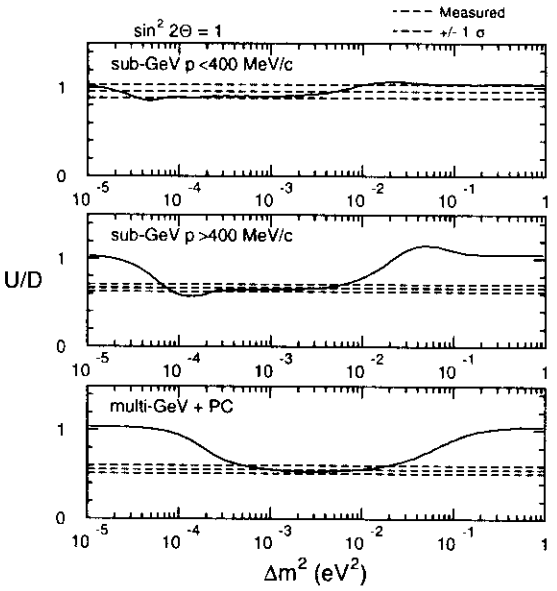

FIG. 36. The expected *Up/Down* (U/D) values for μ-like events and for three momentum ranges are shown as a function of Δm^2 (solid curves). Also shown are the observed U/D values with their errors (dashed lines).

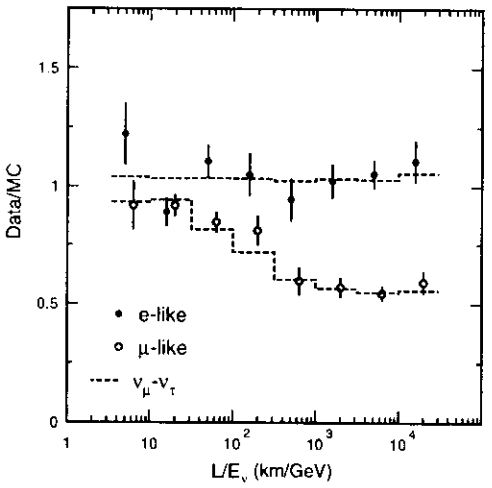

FIG. 37. Data/MC values for e-like and μ-like events as a function of $L(\mathrm{km})/E_\nu(\mathrm{GeV})$. White and black circles show μ-like and e-like data, respectively. The dashed histograms show the prediction with neutrino oscillations ($\Delta m^2 = 2.6\times10^{-3}$ eV^2, $\sin^2 2\theta = 1.0$).

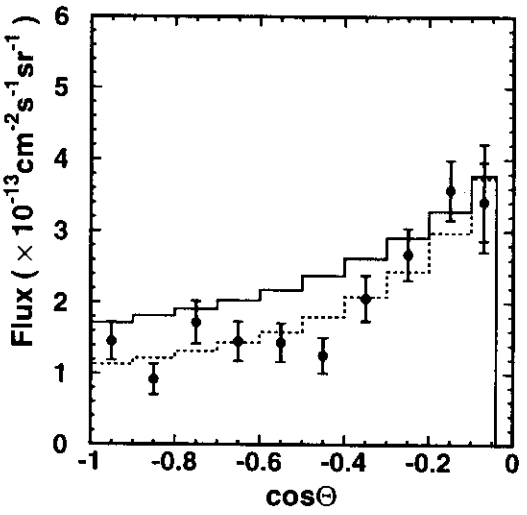

FIG. 38. Zenith angle distribution of the upward through-going muon flux observed in Kamiokande (Hatakeyama *et al.*, 1998). Inner(outer) error bars show statistical (statistical + uncorrelated experimental systematic) errors. The solid histogram shows the expected flux for the null neutrino oscillation case. The dashed histogram shows the expected flux for $\nu_\mu \rightarrow \nu_\tau$ oscillations with ($\sin^2 2\theta$ =1.0, Δm^2 =3.2×10^{-3} eV^2). In the oscillated Monte Carlo, the absolute normalization was adjusted to give the best fit to the data.

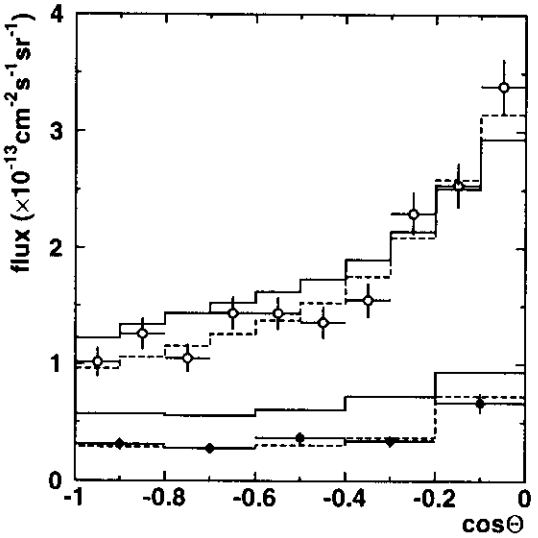

FIG. 39. Zenith angle distribution of the upward through-going muon (blank circles) and stopping muon (black circles) fluxes observed in Super-Kamiokande (Fukuda *et al.*, 1999a, 2000a). Error bars show statistical + uncorrelated experimental systematic errors. Estimated background is subtracted. The solid histograms show the expected fluxes for the null neutrino oscillation case based on the calculated flux of Honda *et al.*, (1995). The dashed histograms show the expected fluxes for $\nu_\mu \rightarrow \nu_\tau$ oscillations with ($\sin^2 2\theta$ =1.0, $\Delta m^2 = 2.8 \times 10^{-3}$ eV^2). In the oscillated Monte Carlo, the absolute normalization was adjusted to give the best fit to the data.

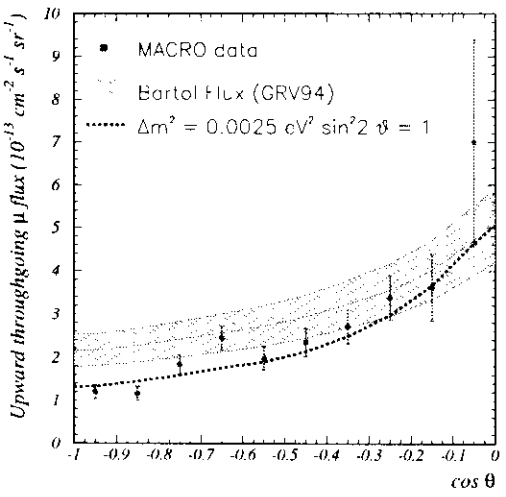

FIG. 40. Zenith angle distribution of the flux of the upward through-going muons with energy higher than 1 GeV observed in MACRO (Ambrosio *et al.*, 1998; Bernardini, 1999; Spurio, 1999). The solid curve shows the expectation for no oscillations and the shaded region shows the absolute normalization uncertainty in the expectation. The dashed line shows the expected flux for $\nu_\mu \rightarrow \nu_\tau$ oscillations with ($\sin^2 2\theta$ =1.0, Δm^2 =2.5×10^{-3} eV^2).

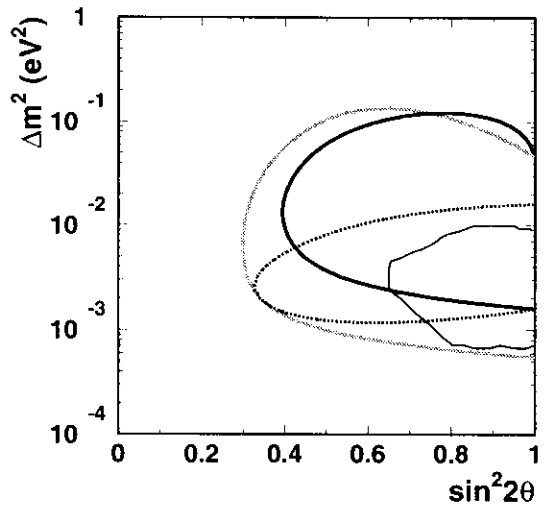

FIG. 41. 90% C.L. allowed regions of the $\nu_\mu \rightarrow \nu_\tau$ neutrino oscillation parameters obtained by upward-going muon data from various experiments. The thick-black, thick-gray and thin-black lines show the regions obtained by upward through-going muons from Super-Kamiokande (Fukuda *et al.*, 1999a, 2000a), Kamiokande (Hatakeyama *et al.*, 1998) and MACRO (Ambrosio *et al.*, 1998; Bernardini, 1999; Spurio, 1999), respectively. The dotted-black curve shows the region obtained by the (stopping/through-going) ratio analysis of upward-going muons from Super-Kamiokande.

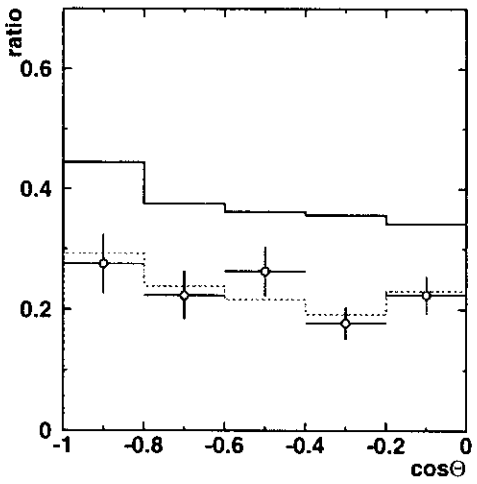

FIG. 42. Zenith angle dependence of the stopping/through-going ratio of the upward going muons obtained by Super-Kamiokande (Fukuda *et al.*, 1999a, 2000a). The solid histogram shows the prediction for the null neutrino oscillation case. The dashed histogram shows the expected ratio for $\nu_\mu \rightarrow \nu_\tau$ oscillations with ($\sin^2 2\theta$ =1.0, $\Delta m^2 = 3.8 \times 10^{-3}$ eV^2).

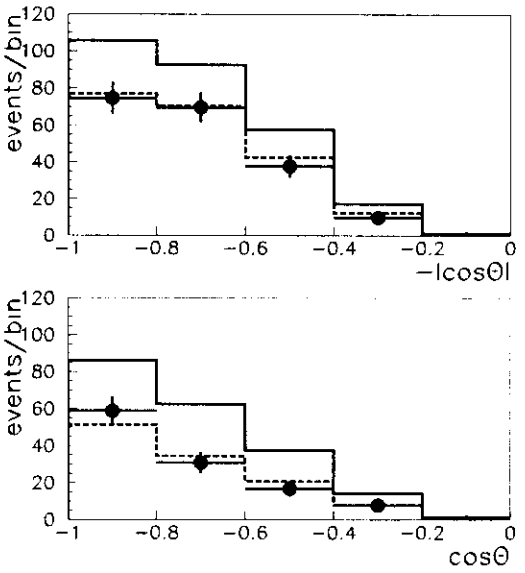

FIG. 43. Zenith angle distributions of (upward stopping muons + downward PC events) (top), and upward PC events (bottom) observed in MACRO (Spurio, 1999). The expected distributions with and without neutrino oscillations are shown by dashed and solid histograms, respectively. For neutrino oscillations, $\nu_\mu \rightarrow \nu_\tau$, $\Delta m^2 = 2.5 \times 10^{-3}$ eV^2 and $\sin^2 2\theta$ =1 are assumed.

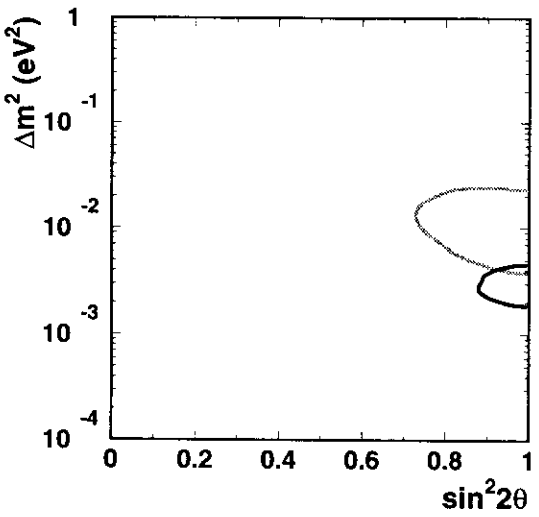

FIG. 44. 90% C.L. allowed region of the $\nu_\mu \rightarrow \nu_\tau$ neutrino oscillation parameters from a combined analysis of fully-contained, partially-contained, upward-stopping muon and upward through-going muon events from Super-Kamiokande (black line, Fukuda *et al.*, 2000a). The result from a combined analysis (without the upward-going stopping muon data) from Kamiokande (gray line, Hatakeyama *et al.*, 1998) is also shown.

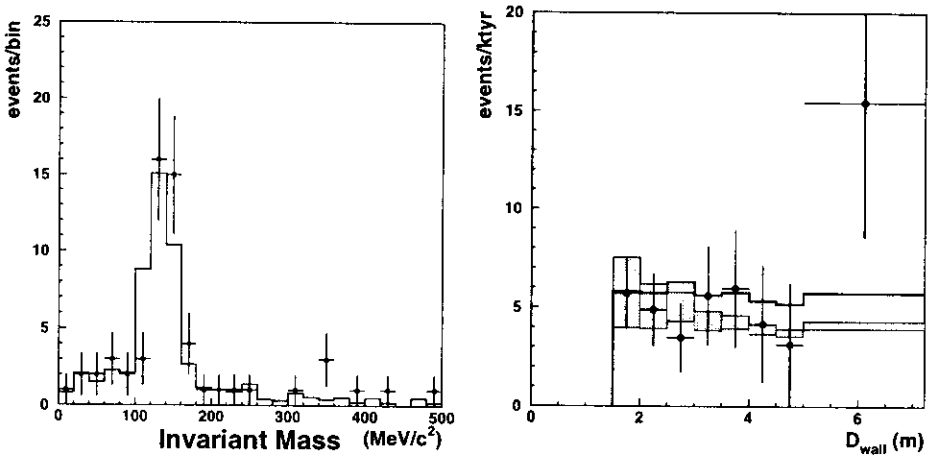

FIG. 45. Left: Invariant mass distribution for atmospheric neutrino data and Monte Carlo events with 2 e-like Cherenkov rings observed in Kamiokande (Fukuda *et al.*, 1996b). The Monte Carlo was normalized by the number of the observed events. Right: Event rate as a function of D_{wall}, the distance to the nearest PMT-plane from the event vertex, for π^0-like events observed in Kamiokande (Fukuda *et al.*, 1996b). The thick histogram shows the MC atmospheric neutrino events. The thin one shows the 90% C.L. upper limit on the neutron plus atmospheric neutrino events, and the shaded area shows the contribution of neutron events to the upper limit histogram. In both cases, the histograms are normalized to the number of data events.

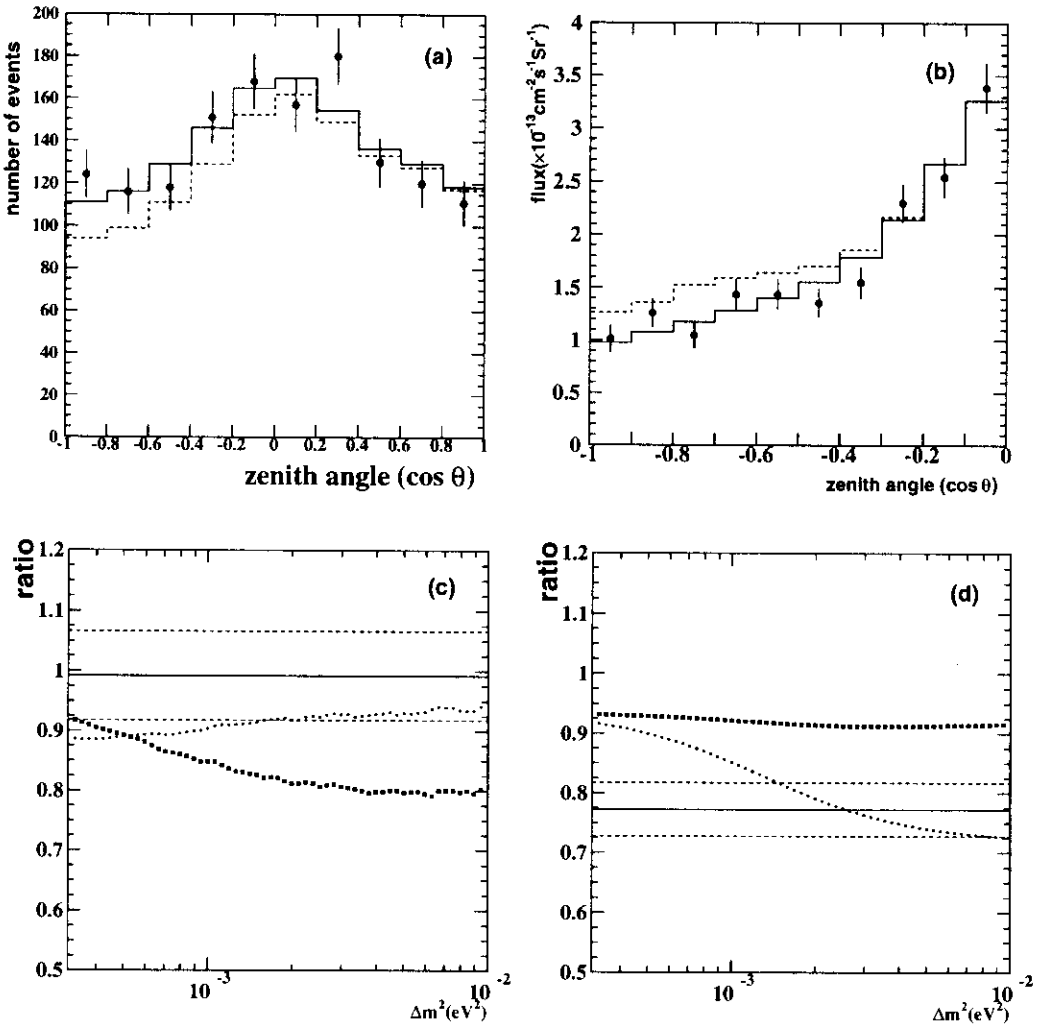

FIG. 46. Zenith angle distributions observed in Super-Kamiokande (Fukuda *et al.*, 2000c) for: (a)multi-ring events with the most energetic ring being e-like and E_{vis} >400 MeV (61 kton-yr), and (b)upward through-going muon events (1074 days). In (a) and (b), solid (dashed) histograms show the expectations for $\nu_\mu \rightarrow \nu_\tau$ ($\nu_\mu \rightarrow \nu_{sterile}$) oscillations. In (c), expected $Up(-1 < cos\Theta < -0.4)/Down(0.4 < cos\Theta < 1)$ ratios of the multi-ring events for $\nu_\mu \rightarrow \nu_\tau$ (thin-dotted line) and $\nu_\mu \rightarrow \nu_{sterile}$ (thick-dotted line) are plotted as a function of Δm^2. Also shown in the same figure is the $Up/Down$ ratio of the data. The solid line shows the central value of the data and the dashed lines show the $\pm 1\sigma$ statistical error. In (d), expected $Vertical(-1 < cos\Theta < -0.4)/Horizontal(-0.4 < cos\Theta < 0)$ ratios of upward through-going muon events for $\nu_\mu \rightarrow \nu_\tau$ (thin-dotted line) and $\nu_\mu \rightarrow \nu_{sterile}$ (thick-dotted lines) are plotted as a function of Δm^2. Also shown in the same figure is the $Vertical/Horizontal$ ratio of the data. In these figures, $\sin^2 2\theta = 1$ is assumed for the expected lines.

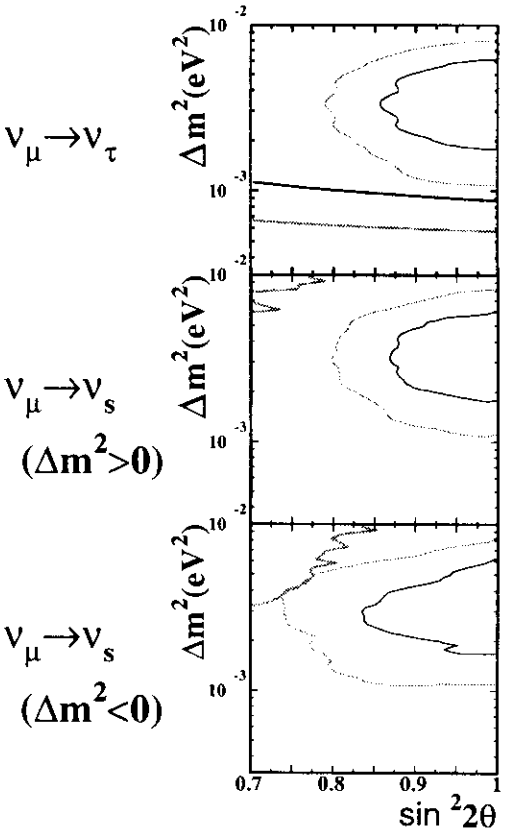

FIG. 47. 90 and 99% C.L. allowed regions of neutrino oscillation parameters obtained by the FC events are shown by the thin-black and thin-gray lines, respectively for $\nu_\mu \rightarrow \nu_\tau$ (top), $\nu_\mu \rightarrow \nu_{sterile}$ ($\Delta m^2 > 0$) (middle), and $\nu_\mu \rightarrow \nu_{sterile}$ ($\Delta m^2 < 0$) (bottom). Also shown are the excluded regions from the combined analysis of the multi-ring, high-energy-PC and upward through-going muon events. Thick-black and thick-gray lines show the preliminary 90% and 99% C.L. exclusion lines, respectively. In each figure, the regions below the thick lines are excluded at 90 or 99% C.L.. In (b) and (c), most of the parameter regions suggested by the FC analysis are disfavored at 99% C.L. (Fukuda *et al.*, 2000c).